Chapter 1
Earth's Climate System

Ross J. Salawitch, Brian F. Bennett, Austin P. Hope, Walter R. Tribett, and Timothy P. Canty

Abstract This chapter provides an overview of the factors that influence Earth's climate. The relation between reconstructions of global mean surface temperature and estimates of atmospheric carbon dioxide (CO_2) over the past 500 million years is first described. Vast variations in climate on geologic time scales, driven by natural fluctuations of CO_2, are readily apparent. We then shift attention to the time period 1765 to present, known as the Anthropocene, during which human activity has strongly influenced atmospheric CO_2, other greenhouse gases (GHGs), and Earth's climate. Two mathematical concepts essential for quantitative understanding of climate change, radiative forcing and global warming potential, are described. Next, fingerprints of the impact of human activity on rising temperature and the abundance of various GHGs over the course of the Anthropocene are presented. We conclude by showing Earth is in the midst of a remarkable transformation. In the past, radiative forcing of climate represented a balance between warming due to rising GHGs and cooling due to the presence of suspended particles (aerosols) in the troposphere. There presently exists considerable uncertainty in the actual magnitude of radiative forcing of climate due to tropospheric aerosols, which has important consequences for our understanding of the climate system. In the future, climate will be driven mainly by GHG warming because aerosol precursors are being effectively removed from pollution sources, due to air quality legislation enacted in response to public health concerns.

Keywords Paleoclimate • Anthropocene • Global warming • Greenhouse gases • Radiative forcing

1.1 Earth's Climate History

Reconstructions of Earth's climate provide a remarkable record of environmental change over vast periods of time. The co-evolution of climate and life on Earth is well established (Schneider 1984; Kasting and Siefert 2002; Sagan and Mullen 1972; Petit et al. 1999). Earth's paleoclimate record is examined here, in some detail, because knowledge of the past is key to understanding the future.

The earliest evidence for life on Earth dates to about 3.5 billion years before present (Bybp) (Brasier et al. 2002). Early life consisted of prokaryotes, one celled bacteria that

R.J. Salawitch et al., *Paris Climate Agreement: Beacon of Hope*,
Springer Climate, DOI 10.1007/978-3-319-46939-3_1

thrived in an oxygen (O_2) free environment. These organisms had no nucleus and reproduced by cell division. The first prokaryotes likely made organic matter by combining carbon dioxide (CO_2) with molecules such as hydrogen sulfide (H_2S), releasing water (H_2O) and elemental sulfur to the environment (Canfield and Raiswell 1999).

Early in Earth's history the favored atmospheric fate for carbon-bearing compounds was methane (CH_4), because the atmosphere was in a state chemists call "reducing". Stellar astronomy indicates that at the time early life formed, the luminosity of our Sun was about 30 % less than today, which should have caused ancient oceans to freeze. As explored in detail throughout this book, CH_4 is a more potent greenhouse gas (GHG) than CO_2. Extremely high levels of atmospheric CH_4 and ammonia (NH_3), another reduced compound that is also a strong GHG, were likely responsible for preventing Earth's ancient oceans from freezing (Sagan and Mullen 1972).

Prokaryotes were the first to develop photosynthesis, the ability to convert sunlight, carbon dioxide (CO_2), and water (H_2O) into glucose $C_6H_{12}O_6$. Eventually, prokaryotic photosynthesis caused atmospheric O_2 to rise from about one part per million of all air molecules to 21 %. Margulis and Sagan (1986) call the initial build-up of atmospheric O_2 the greatest environmental crisis Earth has ever endured. At the time, O_2 was toxic to most life on Earth. As a result, a mass extinction called the Great Oxygenation Event occurred about 2.5 Bybp. One can only imagine the emergency meetings of bacterial communities, seeking to ban their photosynthetic cousins in an effort to halt the build-up of atmospheric O_2.

The rise of atmospheric O_2 had enormous consequences. For the first time in Earth's history, CO_2 was the favored state for atmospheric carbon gases. Conversion of atmospheric CH_4 to CO_2 likely led to Earth's first glaciation event about 2.4 Bybp (Frei et al. 2009). The build-up of O_2 also led to formation of Earth's protective ozone (O_3) layer, which was necessary for life to emerge from sea to land. Finally, the global, atmospheric chemical shock induced by the Great Oxygenation Event facilitated the evolution of eukaryotes: nucleated cells that metabolize O_2. You are made of eukaryotic cells!

Plant life first appeared on land about 500 million years before present (Mybp) (Kenrick and Crane 1997). Even though, as alluded to above, much is known about climate and the state of Earth's atmosphere prior to this time, reconstructions of global variations in Earth's climate and atmospheric CO_2 are only available for the most recent 500 million years.

Figure 1.1 shows the variations in the global mean surface temperature and the abundance of carbon dioxide (CO_2) over the past 500 million years. The temperature estimates are anomalies (ΔT) with respect to the mean state of Earth's climate that existed during recent pre-industrial time (i.e., years 1850–1900). Notable events regarding the evolution of life (Dinosaurs, Rise of Mammals, etc.) are indicated to the left and phenomenon regarding the global carbon cycle and climate (Rise of Forests, Greenland Glaciation, etc.) are marked to the right. This figure is our composite of a considerable number of paleoclimatic studies, as described in Methods. To facilitate discussion of this figure, six Eras are denoted. These should not be confused with the formal use of the word Era by Geologists. Each era in Fig. 1.1 spans a different length of time; the interval over which Dinosaurs lived (about 230–65 Mybp) is about 2.5 times longer than the time between the Rise of Mammals and present.

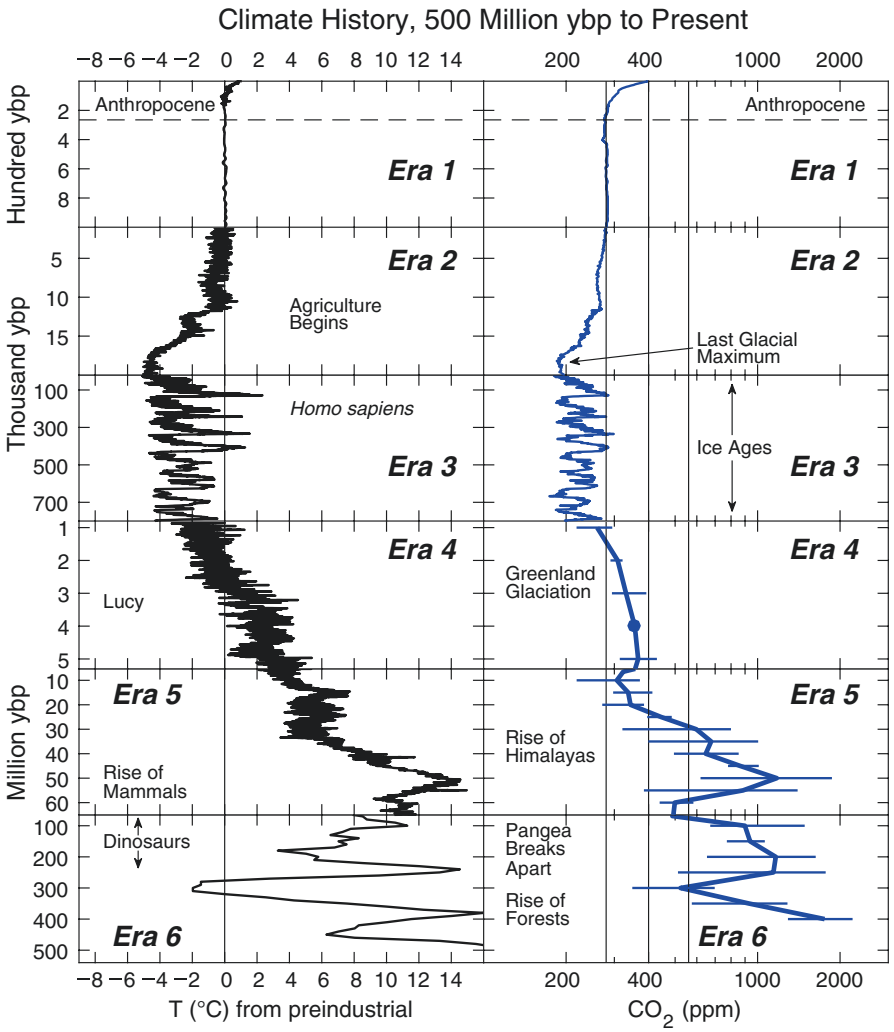

Fig. 1.1 Earth's climate history, past 500 million years. Historical evolution of global mean surface temperature anomaly (ΔT) relative to a pre-industrial baseline (i.e., mean value of global temperate over 1850–1900) (*left*) and the atmospheric mixing ratio of CO_2 (*right*). Major events in the evolution of life on Earth as well as either changes in climate of the global carbon cycle are denoted. The *vertical line* on the ΔT panel at zero marks the pre-industrial baseline; the *vertical lines* on the CO_2 panel denote mixing ratios of 280 ppm (pre-industrial), 400 ppm (current level) and 560 ppm (twice pre-industrial level). These time series are based on hundreds of studies; see Methods for further information

Figure 1.1 shows that Earth has undergone vast changes in climate as well as the abundance of atmospheric CO_2. A logarithmic scale is used to represent the mixing ratio of atmospheric CO_2, because the radiative forcing of climate (see Sect. 1.2.1) is proportional to the logarithm of CO_2. Figure 1.1 shows, clearly and beyond debate, the strong association of Earth's climate and atmospheric CO_2. Looking backwards in time, as CO_2 rises, Earth warms.

On geological time scales, atmospheric CO_2 is controlled by the carbonate-silicate cycle (Berner et al. 1983). Atmospheric supply of CO_2 occurs during volcanic eruptions and hydrothermal venting. Atmospheric removal of CO_2 is more complicated. The weathering of minerals converts atmospheric CO_2 into a water soluble form of carbon; ocean organisms incorporate soluble carbon into their shells and, when these animals perish, their shells sink to the ocean floor. Plate tectonics buries the sinking sediment, after which the carbon either remains in Earth's mantle or, on occasion, is spewed back to the atmosphere-ocean system, via either volcanoes or deep sea vents.

The first dramatic perturbation to the carbonate-silicate cycle was induced by the rise of forests. About 500 Mybp, atmospheric CO_2 may have been as high as 5000 parts per million by volume (ppm), more than a factor of 10 larger than today (Fig. 1.1) (Berner 1997). Of course, Earth was also exceedingly warm compared to today. The first plants to evolve, bryophytes, were algae-like organisms that probably eased the transition from sea to land by finding homes on moist rocky surfaces. Bryophytes are known as non-vascular plants; they lack roots to transport moisture. Moss is a modern-day bryophyte. Vascular pteridophytes (fern-like organisms) evolved about 500 Mybp, soon leading to the rise of forests. This resulted in a steady, dramatic decline in atmospheric CO_2 because early forests lacked the abundant bacteria, fungi, and small soil animals that recycle plant matter in contemporary forests. Carbon in the forests that prevailed during the time depicted as Era 6 of Fig. 1.1 was buried and converted to modern day coal and natural gas deposits, due to the intense heat and pressure within Earth's mantle. This carbon is now being released back to the atmosphere–ocean system, perhaps to generate the electricity used to help you read this book.

The next event that transformed the global carbon cycle was the rise of the Himalayas (Raymo and Ruddiman 1992). During the period of time depicted in Era 5, plate tectonics resulted in the formation of the modern-day continents. The exposure of fresh minerals due to the vast tectonic activity associated with formation of the Himalayan mountain range, the largest in the world, led to the steady draw down of CO_2 and associated cooling depicted in Era 5 of Fig. 1.1.

About 3 Mybp, two remarkable events occurred. Our predecessor Lucy (*Australopithecus afarensis*) roamed modern day Ethiopia (Johanson and White 1979). At about the same time, Greenland first became glaciated (Lunt et al. 2008). While the emergence of an early human ancestor who walked in an upright manner is in no way related to the glaciation of Greenland, it is worth noting that global mean surface temperature and atmospheric CO_2 at the time of Lucy were both estimated to be at modern, pre-industrial levels (Era 4, Fig. 1.1).

The most compelling association of CO_2 and climate is provided by the covariance of these quantities during the past 800,000 years (Era 3, Fig. 1.1) (Imbrie and Imbrie 1979). Earth's climate oscillated between glaciated and inter-glacial states, with atmospheric CO_2 levels of about 200 ppm and 280 ppm, respectively, characterizing each state (Barnola et al. 1987). Lower levels of atmospheric CO_2 prevailed during glacial times due to more productive ocean biogeochemical uptake (Marino et al. 1992), perhaps facilitated by the oceanic supply of iron resulting from the grinding of glaciers on rock (Martin 1990). The ultimate pace-maker of these cycles is orbital variations of Earth about the Sun, known as Milankovitch cycles (Imbrie and Imbrie 1979).

The precise timing of the rise and fall of temperature and CO_2 during Era 3 of Fig. 1.1 is a source of considerable dispute between the climate "believers" and "deniers". The initial, literal interpretation of the ice core record suggested that changes in temperature proceeded variations in CO_2 by about 800 years (Caillon et al. 2003). If so, the deniers argue, then CO_2 is responding to, rather than driving, global climate change. It is essential to appreciate that: the ice core record of CO_2 is discerned by measuring the composition of bubbles trapped in ice; historic temperature is quantified by measuring isotopic composition of the hydrogen and/or oxygen elements within the ice; and bubbles within the sampled ice cores move with respect to the surrounding ice over geologic time. A recent re-analysis of the timing of variations in temperature and CO_2 of an Antarctic ice core, which considers movement of bubbles with respect to the surrounding ice, reveals synchronous variation within the uncertainty of measurement (Parrenin et al. 2013). This interpretation supports the view that changes in atmospheric CO_2 did indeed drive glacial/interglacial transitions.

Ancient air preserved in ice cores reveals that when Earth underwent glacial conditions during Era 3 of Fig. 1.1, atmospheric CH_4 fell to about 0.4 ppm. During interglacial periods, atmospheric CH_4 reached a value of 0.7 ppm (Petit et al. 1999; Loulergue et al. 2008). Natural sources of CH_4 vary by an amount large enough to induce considerable variations in atmospheric abundance, with some consequence for the radiative forcing of climate. Methane is released to the atmosphere when frequently flooded regions (wetlands) experience low oxygen (anaerobic) conditions. It is likely that the higher levels of CH_4 during warm epochs was due to a larger preponderance of wetlands, particularly in the northern hemisphere (NH), as these regions went from ice-covered to ice-free as Earth transitioned from glacial to interglacial conditions (Brook et al. 2000; Sowers 2006). Variations in atmospheric CH_4 also played a role in driving glacial/interglacial climate cycles.

The correlation of temperature and atmospheric CO_2 over vast periods of Earth's history is firmly established by the hundreds of studies that have led to our composite Fig. 1.1. Of course, correlation does not necessarily imply causation. The radiative forcing of climate due to CO_2 and other GHGs is explored in great detail later in this chapter.

Modern Homo sapiens evolved about 200,000 years ago and left Africa about 100,000 years ago (Carto et al. 2009). The paths of early humans were influenced by various rapid climate change events that took place at the end of Era 3 and the start of Era 2 of Fig. 1.1. During the height of most recent glaciation, about 20,000 years ago, modern day Manhattan was under a sheet of ice nearly half a mile thick and global sea level was 120–130 m (about 400 ft!) lower than today. Human settlement of North America hugged the coastline, as the interior was inhospitable if not impassable. Scandinavia, England, Wales, Scotland, and Ireland were similarly buried under year-long ice.

Modern agriculture was invented during the Neolithic Revolution, about 12,500 years ago. The Earth was in the midst of climatic warming following the end of the last ice age, which has been implicated as a causal factor because the domestication of plants and animals occurred nearly simultaneously at places separated by great distance (Gepts and Papa 2001). Agriculture flourished, population grew, and humans colonized all parts of the Earth (except Antarctica) during the climatically quiescent times depicted at the end of Era 2 and start of Era 1 in Fig. 1.1.

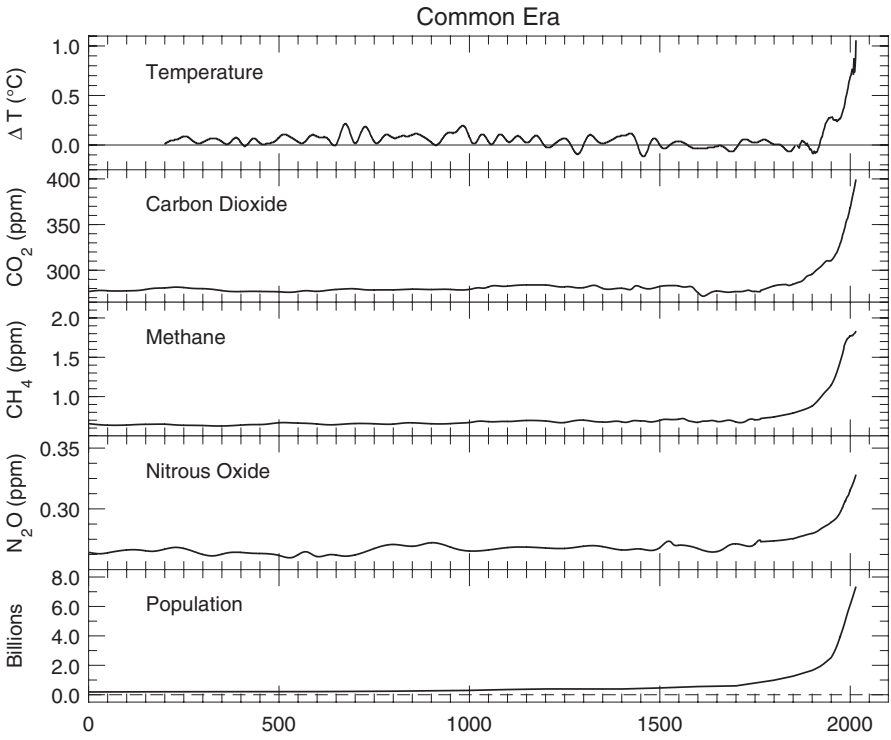

Fig. 1.2 Temperature, GHGs, and population, Common Era. Time series of Earth's global mean surface temperature anomaly (ΔT) relative to pre-industrial baseline (1850–1900 mean) (Jones and Mann 2004; Jones et al. 2012), the atmospheric mixing ratio of CO_2, CH_4, and N_2O (MacFarling Meure et al. 2006; Ballantyne et al. 2012; Dlugokencky et al. 2009; Montzka et al. 2011) and global population (Klein Goldewijk et al. 2010; United Nations 2015) over the Common Era. See Methods for further information

Eventually, population rose to an extent that humans began to exert a measurable effect on the GHG levels of the atmosphere, a time period now known as the Anthropocene (Crutzen and Stoermer 2000). Figure 1.2 illustrates the time evolution of ΔT, CO_2, CH_4, nitrous oxide (N_2O), and population during the past 2000 years, the so-called Common Era. The association of the rise in population and increased atmospheric levels of CO_2, CH_4, and N_2O is again irrefutable. Before delving into the Anthropocene, we shall comment on one more controversy.

Europe experienced unusually warm temperatures from about 950–1250 AD, a time known as the Medieval Warm Period (MWP) (Moberg et al. 2005). Our Fig. 1.2, which relies on the ***global*** temperature reconstruction of Jones and Mann (2004), does not depict the MWP. The study of Jones and Mann (2004) suggests the MWP was regional in nature, with little to no global expression. The temperature record in Fig. 1.2, which has become known as "The Hockey Stick", has led to considerable controversy. One account is described in the book *The Hockey Stick and the Climate Wars*: *Dispatches from the Front Lines* (Mann 2012). In 2006, the

United States National Academy of Sciences (NAS 2006) reviewed the voluminous literature on climate reconstructions over the Common Era and concluded:

> Based on the analyses presented in the original papers by Mann et al. and this newer supporting evidence, the committee finds it plausible that the Northern Hemisphere was warmer during the last few decades of the 20th century than during any comparable period over the preceding millennium. The substantial uncertainties currently present in the quantitative assessment of large-scale surface temperature changes prior to about A.D. 1600 lower our confidence in this conclusion compared to the high level of confidence we place in the Little Ice Age cooling and 20th century warming. Even less confidence can be placed in the original conclusions by Mann et al. (1999) that 'the 1990s are likely the warmest decade, and 1998 the warmest year, in at least a millennium' because the uncertainties inherent in temperature reconstructions for individual years and decades are larger than those for longer time periods and because not all of the available proxies record temperature information on such short timescales.

This NAS statement provides fodder for both the believers and deniers. The deniers posit that if global temperature was indeed unusually warm from 950 to 1250 AD, at a time when CO_2, CH_4, and N_2O were known to be stable (Fig. 1.2), then other factors such as solar luminosity must be responsible. If so, the argument goes, then perhaps the late twentieth century and early twenty-first century warming is due to some factor other than anthropogenic GHGs.

A recent study of ocean heat content supports the view that the higher temperature of the MWP was indeed global in nature (Rosenthal et al. 2013), similar to the conclusion reached by Soon and Baliunas (2003) a decade earlier. If so, then the time series of ΔT shown in Fig. 1.2 is in need of revision. Regardless, as shown below, extremely strong scientific evidence implicates GHGs produced by human activities as the primary driver of rising global temperature during the past half-century.

1.2 The Anthropocene

The Anthropocene refers to the recent interval during which the atmospheric abundance of GHGs that drive Earth's climate have increased due to human activity (Crutzen and Stoermer 2000). Most peg the start of the Anthropocene to the mid-eighteenth century, linked to the invention of the steam engine by James Watt in 1784 (Steffen et al. 2015). Others suggest humans have had a discernable influence on GHGs for a much longer period of time, and argue for a start date to the Anthropocene as far back as 8000 years before present (ybp) (Ruddiman 2003).

We use 1765 as the start of the Anthropocene for several reasons. The largest influence of humans on GHGs has certainly occurred since 1765. Estimates of radiative forcing of climate (defined in Sect. 1.2.1) due to a wide variety of human activities based on a multi-year effort of scientists from many nations, are available in a transparent, easily accessible format[1] back to 1765 (Meinshausen et al. 2011).

[1] RF estimates in ASCII and Excel format are available at:
http://www.pik-potsdam.de/~mmalte/rcps/data/20THCENTURY_MIDYEAR_RADFORCING.DAT
http://www.pik-potsdam.de/~mmalte/rcps/data/20THCENTURY_MIDYEAR_RADFORCING.xls

Finally, changes in global mean surface temperature, to which RF of climate will be related, are much more certain from 1765 to present than for times extending back to the invention of agriculture (NAS 2006). Our choice is not meant to dismiss the importance of human influence on climate prior to 1765. If, as suggested by Ruddiman (2003), human activity 8000 ybp did indeed offset the onset of extensive glaciation due to declining summer insolation at Northern high latitudes (driven by Milankovitch orbital variations), this would be a fascinating benefit of human ingenuity, especially for indigenous peoples of high northerly latitudes.

Rather than wade deeper into the debate over the start of the Anthropocene, we next describe a few figures that illustrate the human fingerprint on the global carbon cycle and climate change over the past several centuries. Along the way, the mathematical principles needed to understand the material presented in Chaps. 2 and 3 are developed.

1.2.1 Radiative Forcing

In the absence of an atmosphere, the temperature of Earth would be governed by:

$$T_{EARTH} = \left(\frac{(1 - Albedo) S/4}{\sigma} \right)^{\frac{1}{4}} \tag{1.1}$$

Albedo, the Latin word for whiteness, refers to the fraction of incoming sunlight reflected to space (commonly about 0.3 (or 30 %) for Earth), S is the luminosity of our Sun at the distance of Earth's orbit (1370 W m^{-2}), and σ is the Stefan Boltzmann constant (5.67×10^{-8} W m^{-2} K^{-4}). A value of $S/4$ is used because the Earth intercepts sunlight like a disk and radiates heat like a sphere; 1/4 is the ratio of the surface area of a disk to that of a sphere (this concept as well as Eq. 1.1 are explained in many introductory Earth Science textbooks). Solving for the putative temperature of planet Earth without an atmosphere yields 255 K, which is −18° Celsius (°C) or 0° Fahrenheit (°F). This is much colder than the average temperature of today's Earth. If the temperature found using Eq. 1.1 actually applied, our oceans would be frozen.

The greenhouse effect, the trapping of radiation by our planet's atmosphere, is responsible for the difference between the Earth's actual temperature and that found using Eq. 1.1. Earth's mean surface temperature is about 15.5 °C or 60 °F. Earth's atmosphere is responsible for increasing the amount of energy the surface receives, by several hundred W m^{-2}, in comparison to an Earth devoid of an atmosphere. This excess heat is driven by the abundance and molecular properties of GHGs such as H_2O, CO_2, CH_4, and N_2O, as well as clouds (i.e., condensed H_2O droplets).

Infrared radiation (or heat in the form of photons) emitted by Earth's surface is resonant with various vibrational modes of GHG molecules, inducing these photons to be absorbed and re-emitted in all directions. Some of this absorbed and re-emitted radiation is sent back to the surface. As such, GHGs in Earth's atmosphere act as a blanket, trapping heat that would otherwise escape to space. Water vapor, the most

important GHG, is responsible for the majority of radiation sent back to the surface. The abundance of H_2O in our atmosphere is controlled by thermodynamics: i.e., the evaporation of H_2O from the oceans, condensation of H_2O in the atmosphere to form clouds, and deposition of H_2O back to the surface in the form of precipitation. Atmospheric H_2O varied prior to the onset of human influence; the effect of thermodynamics on various isotopes of H_2O preserved in ice cores is an important tool for quantitative reconstruction of past climate (Jouzel et al. 1987).

The radiative forcing (RF) of climate refers to the increase in the amount of heat directed to Earth's lower atmosphere as the abundance of GHGs rise. Here and throughout this book, we follow the convention established in the 2001 Intergovernmental Panel on Climate Change (IPCC) Physical Science Basic Report (IPCC 2001) that RF of climate is defined as the change in the net flow of energy (sunlight plus infrared heat) at the tropopause (boundary between the lower atmosphere, or troposphere, and the upper atmosphere, or stratosphere) relative to a particular start date, after allowing for stratospheric temperatures to adjust to radiative equilibrium. This concept is explained well in Sect. 2.2 of IPCC (2007).

Figure 1.3a shows several time series of the RF of climate over the Anthropocene. The curves are set to zero in year 1765 and represent changes relative to this start time,

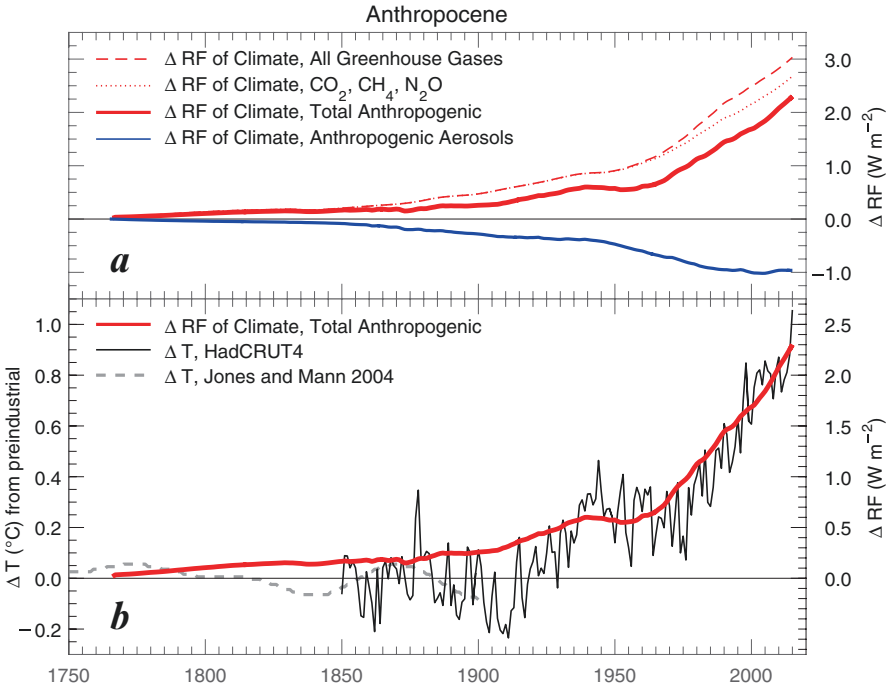

Fig. 1.3 Radiative forcing of climate and temperature, Anthropocene. (**a**) change in the radiative forcing of climate (ΔRF) relative to year 1765, from various factors (as indicated) for the RCP 4.5 scenario (Meinshausen et al. 2011); (**b**) total anthropogenic ΔRF (*red*) and the global mean surface temperature anomaly (ΔT) relative to pre-industrial baseline (1850–1900 mean) from the modern instrument record (HadCRUT4) (Jones et al. 2012) and from various proxies (Jones and Mann 2004). See Methods for further information

hence they are denoted ΔRF.[2] Red is used to represent warming (positive ΔRF); blue is used to show cooling (negative ΔRF). These ΔRF curves are based on the GHG and aerosol precursor abundances used to drive climate model simulations of IPCC (2013). The RF of climate due to human release of CO_2, CH_4, and N_2O is the primary focus of this book. The historic ΔRF due to all anthropogenic GHGs (dashed red) exceeds that of the CO_2/CH_4/N_2O triplet (dotted red) by a small amount, with most of the difference due to a class of compounds called Ozone Depleting Substances (ODS). Even though ODS exhibit a greenhouse effect, they are generally not labeled as GHGs because their most important detrimental effect is depletion of Earth's ozone layer. Also, industrial production of ODS has been successfully curtailed by the Montreal Protocol and the effect of these compounds on climate will diminish in the future (WMO 2014).

The human release of pollutants that increase the burden of small particles in the troposphere, known as aerosols, leads to a reduction in the RF of climate (blue line, Fig. 1.3a). This occurs because many aerosols reflect sunlight. An estimate of ΔRF due to aerosols provided by Meinshausen et al. (2011) is shown in Fig. 1.3a.[3] As detailed below, there is considerable uncertainty in this term.

The total ΔRF due to human activity is shown by the solid red curve in Fig. 1.3a, b. All told, human activities have increased the RF of climate by about 2.3 W m^{-2} between 1750 and present. Figure 1.3b shows that the time variation of total ΔRF due to humans (red line) closely resembles the observed rise in global mean surface temperature anomaly (black and grey lines). Below we conduct quantitative analysis of these two quantities, both within this chapter as well as throughout Chap. 2.

Figure 1.4 details the change in RF of climate, between 1750 and 2011, due to various factors.[4] Numerical values are from Chap. 8 of IPCC (2013). Error bars denote the 5 and 95 % confidence intervals for each quantity. Processes that effect RF of climate but are not regulated under GHG legislation, such as Stratospheric and Tropospheric Ozone and Land Use Change, as well as minor terms such as Contrails and Solar Irradiance, are also shown. The solid red lines of Fig. 1.3 consider all of the terms shown in Fig. 1.4.

There are several aspects of Fig. 1.4 worth emphasizing. Human release of GHGs has warmed climate, with CO_2 being the most important contributor. The combined effect of the two other most important long-lived anthropogenic GHGs (CH_4, N_2O) plus all of the ODS compounds has enhanced this CO_2-based warming by about 60 %. Tropospheric ozone (O_3), a pollutant harmful to human health and agriculture, has warmed climate over the course of the Anthropocene by nearly as much as CH_4. Tropospheric O_3 is regulated by air quality regulations that vary by country and focus

[2] Delta is the first letter of the Greek word diaphorá, which means difference. Scientists often use either Δ (capital delta) or δ (lowercase delta) to represent difference. The ΔRF data in Fig. 1.3 start in 1765 because this is the first year for which numerical values are available (see Methods).

[3] The blue line is the combination of the three terms: the direct radiative effect of aerosols, the perturbation to the reflectivity of clouds induced by aerosols, and the darkening of snow caused by the deposition of black carbon. This estimate includes the following types of aerosols: sulfate, nitrate, mineral dust, as well as organic carbon and black carbon from both fossil fuel combustion and biomass burning.

[4] Figure 1.3 spans 1765–2011 whereas Fig. 1.4 tabulates ΔRF between 1750 and 2011. The different start years are a result of how scientists who worked on IPCC (2013) handled various data streams. This difference is inconsequential since human activity imposed very little influence on ΔRF between 1750 and 1765.

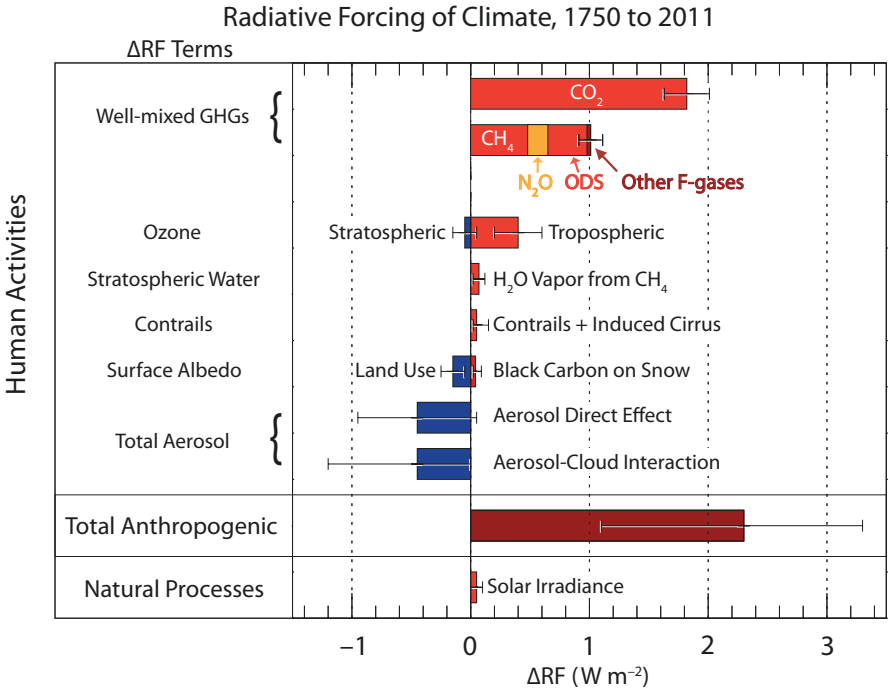

Fig. 1.4 Radiative forcing of climate, various factors, Anthropocene. Change in radiative forcing of climate (ΔRF) over the course of the Anthropocene (in this case, 1750–2011) due to human factors (GHGs and aerosols) and natural processes (solar irradiance). Error bars represent the 5–95 % confidence interval. The ODS entry represents ΔRF due to ozone depleting substances such as CFC-11, CFC-12, etc. The Other F-gases entry represents ΔRF due to HFCs, PFCs, SF_6, and NF_3. Numerical estimates for ΔRF are shown when available; otherwise, numerical estimates for the change in Effective Radiative Forcing (ΔERF) are used. After Fig. 8.15 of IPCC (2013). See Methods for further information

on surface conditions (i.e., the air we breathe). There is no coordinated international effort to limit future growth of tropospheric O_3. Human release of pollutants that lead to formation of tropospheric aerosols causes climate to cool due to two processes nearly equal in magnitude but having large uncertainty: the reflection of sunlight by aerosols (Aerosol Direct Effect) and the effect of aerosols on cloud formation (Aerosol-Cloud Interaction).[5] The net effect of all human activity on ΔRF (bar labeled Total Anthropogenic) is about 25 % larger than ΔRF due to CO_2 and has a considerably larger uncertainty (size of respective error bars) (Chap. 8, IPCC (2013)).

Other aspects of global warming are represented in Fig. 1.4. The reflectivity of Earth's surface has changed primarily due to deforestation that makes the surface

[5] The effect of anthropogenic aerosols on the radiative properties of clouds is different, from a climate modeling perspective, than the evolution of cloud properties as the surface warms. Specialists refer to the former as the aerosol indirect effect and the latter as cloud feedback. A considerable research effort informs us that the aerosol indirect effect leads to a cooling (negative RF) of uncertain magnitude and the cloud feedback could either lead to warming or cooling.

brighter (leading to cooling) and the deposition of dark, carbonaceous material on snow that darkens the surface (leading to warming). Contrails from aircraft have led to a slight warming, mainly because of induced clouds. A slight warming term is also attributed to an increase in stratospheric humidity driven by rising tropospheric CH_4, which is converted to H_2O when lost in the stratosphere. The depletion of stratospheric O_3 has resulted in slight cooling. Finally and most importantly, scientists have been able to estimate the time variation of total solar irradiance over the course of the Anthropocene. The trend in solar irradiance over this two and a half century time period is small. Even if the MWP discussed above turns out to be as warm as the present decades, presumably due to an increase in solar irradiance during the middle of the Common Era (Bard et al. 2000), scientists are nonetheless confident the rise in temperature over the Anthropocene was driven by rising GHGs and not a change in the luminosity of our Sun (Chap. 8, IPCC (2013)).

1.2.2 Global Warming Potential

The global warming potential (GWP) metric was developed to guide public policy decisions regarding trade-offs of release of various GHGs. The GWP of a particular compound represents the ratio of the rise in global mean surface temperature (GMST) due to the release of a particular amount (mass) of this compound, relative to the rise in GMST resulting from the release of the same amount (mass) of CO_2. Inherent in the computation of GWP is that the increase in GMST is found over a particular time horizon.

The most commonly used time horizons are 20 and 100 years. The mathematical expression for the GWP of CH_4 over a 100-year time horizon, which relies on the use of a calculus concept called integration, is given by:

$$GWP\left(\mathrm{CH}_4\right)=\frac{\int_0^{100\,\mathrm{yrs}} a_{\mathrm{CH}_4}\times \mathrm{CH}_4\left(t\right)dt}{\int_0^{100\,\mathrm{yrs}} a_{\mathrm{CO}_2}\times \mathrm{CO}_2\left(t\right)dt} \tag{1.2}$$

where a_{CH_4} and a_{CO_2} are the radiative efficiencies (units W m^{-2} kg^{-1}) of CH_4 and CO_2, respectively, and $CH_4(t)$ and $CO_2(t)$ represent the time dependent response to the release into the atmosphere of the same mass of these two GHGs.[6] The atmospheric lifetime of a GHG denotes the time it takes for a pulsed release of the gas to decay by $1/e$ of the initial value, where $e \approx 2.718$. The lifetimes of CH_4

[6] Equation 1.2 represents a computer simulation of the cumulative radiative forcing of climate over a 100 year time period due to release of a pulse of a certain amount (mass) of CH_4, divided by the cumulative radiative forcing over the same time period due to simulated release of the same amount of CO_2. Since the pulse of CH_4 decays faster than the pulse of CO_2, due to the shorter lifetime of CH_4, the GWP of CH_4 is larger when shorter time periods are considered.

Table 1.1 Global warming potentials

GHG	IPCC (1995)	IPCC (2001)	IPCC (2007)	IPCC (2013)
100-Year time horizon				
CH_4	21	23	25	28, 34[a]
N_2O	310	296	298	265, 298[a]
20-Year time horizon				
CH_4	56	62	72	84, 86[a]
N_2O	280	275	289	264, 268[a]

[a]Allowing for carbon cycle feedback

and N_2O used in IPCC (2013) calculation of GWP are 12.4 and 121 years, respectively. These lifetimes are typically used for evaluation of the numerator of Eq. 1.2, as most GWP estimates assume pure exponential decay. Conversely, the decay of the pulse of CO_2 in the denominator of Eq. 1.2 is found using a computer model of the global carbon cycle.

As shown in Chap. 3, the GWP of various GHGs is vitally important for assessing the efficacy of the Paris Climate Agreement[7]. Table 1.1 provides the GWP of CH_4 and N_2O from the past 4 IPCC reports. The GWP of GHGs has been updated over time due to evolving knowledge of the radiative efficiencies and lifetimes of atmospheric compounds. Also, IPCC (2013) provided two values of GWP for CH_4 and N_2O: with and without consideration of carbon cycle feedback.

The most commonly used GWPs for public policy are those found for a 100-year time horizon. This preference is traceable to the 1997 Kyoto Protocol of the United Nations Framework Convention on Climate Change (UNFCCC), which was based on 100-year GWPs. Furthermore, since the values of GWP given in IPCC (2013) that do not allow for carbon cycle feedback are most analogous to values of GWPs given in prior IPCC reports, we will use GWPs for CH_4 and N_2O of 28 and 265, respectively, in our analysis of the Paris Climate Agreement. The GWPs of other GHGs used in our analysis are based on Chap. 8 of IPCC (2013).

The fact that the GWPs of CH_4 and N_2O are much larger than 1 means that, on a per mass basis, these GHGs are considerably more potent than CO_2.[8] Furthermore, the GWP of CH_4 is much larger over a 20-year horizon than a 100-year time horizon, due to the 12.4 year lifetime for CH_4 used in the calculation of GWP. Integrated over 20

[7] The Paris Climate Agreement was negotiated at the 21st Conference of the Parties (COP21) held in Paris, France during December 2015. The COP meetings are an annual gathering of representatives from participating nations, environmental agencies, and industry to address concerns of climate change. For more information see: http://unfccc.int/paris_agreement/items/9485.php

[8] Some textbooks and reports provide GWP values on a per molecule basis, rather than a per mass basis. A molecule of CO_2 with atomic mass of 44 weighs 2.75 times a molecule of CH_4 (atomic mass of 16). Using the IPCC (2013) value for the GWP of CH_4 on a 100 year time horizon, without consideration of carbon cycle feedback, scientists would state CH_4 is 28 times more potent than CO_2 on a *per mass* basis and, at the same time, is 10.2 ($28 \div 2.75$) times more potent than CO_2 on a *per molecule* basis.

years, a significant fraction of the initial, pulsed release of CH_4 is present in the modeled atmosphere. However, integrated over 100 years, a much smaller fraction is present. As discussed in Chap. 4, controlling inadvertent release of CH_4 to the atmosphere will likely be vitally important for reaching the goals of the Paris Climate Agreement, keeping warming well below 2.0 °C and aiming to limit warming to 1.5 °C. The importance of CH_4 would be amplified by a factor of 3 (ratio of 84/28 from Table 1.1) if climate change over a 20-year time horizon were used to guide public policy, placing even more stringent controls on the atmospheric release of this GHG.

Carbon dioxide is the most important anthropogenic GHG for RF of climate (Figs. 1.3a and 1.4), despite the more potent nature of CH_4 and N_2O, because human society has released to the atmosphere a much greater mass of CO_2 than other GHGs. Simply put, CO_2 is the greatest waste-product of modern society. We now turn our attention towards the human fingerprints on global warming as well as on the atmospheric build-up of CO_2 and other GHGs.

1.2.3 Human Fingerprints

As described in Sect. 1.1, Earth's climate has undergone vast variations on geologic time scales. Many of these climate shifts are directly tied to changes in atmospheric CO_2. Studies of paleoclimate must also consider effects on global mean surface temperature (GMST) of continental plate alignment (Hay et al. 1990), the seasonal distribution of sunlight related to variations of Earth's orbit (Erb et al. 2013), as well as the radiative forcing of climate due to aerosols (Chylek and Lohmann 2008) and GHGs other than CO_2 (Sagan and Mullen 1972).

Even though Earth's climate and the abundance of GHGs co-vary on geologic time scales due to natural processes, a scientific consensus has nonetheless emerged that the recent rise in GMST as well as atmospheric burdens of CO_2, CH_4, and N_2O are all driven by human activities (IPCC 2013). Here we briefly review some of the most important human fingerprints on temperature and GHGs. To place the material that follows in the proper perspective, it is important to understand that the time scales involved with geologic change and human history are enormously different. For instance, the ratio of the time since the rise of forests (400 Mypb) to the time since the advent of agriculture (~12,000 ybp) is enormous. If time on Earth since the rise of forests were compressed into a 24 h day, the time since the advent of agriculture would take 2.6 s, which is less than the time it takes to read this sentence!

1.2.3.1 Rising Temperature

As noted above, correlation does not demonstrate causation. We shall first examine the quantitative relation between the rise in the GMST anomaly (ΔT) shown in Fig. 1.3 and the change in radiative forcing of climate (ΔRF) attributed to humans over the Anthropocene.

The Stefan-Boltzmann equation relates the temperature of an object to the rate at which it is able to disperse energy:

$$Power = \sigma T^4 \tag{1.3}$$

Power is used in Eq. 1.3 since *Power* is defined as *Energy*/*Time*, and the Stefan-Boltzmann equation is based on the rate at which energy is dispersed; σ is the same constant used in Eq. 1.1. In equilibrium, Earth's surface releases (or radiates) energy at the same rate it is supplied to the surface by the atmosphere. Hence *Power* in Eq. 1.3 can be replaced with RF, where RF represents the atmospheric radiative forcing of climate:

$$RF = \sigma T^4 \tag{1.4}$$

Those who have taken calculus will understand that upon taking the derivative of Eq. 1.4 and re-arranging terms, it can be shown that:

$$\Delta T = \frac{1}{4\sigma T^3} \Delta RF \tag{1.5}$$

where ΔRF represents a perturbation to the system (i.e., the rise in RF of climate due to human release of GHGs) and ΔT represents the response (i.e., resulting rise in global mean surface temperature).

Scientists use relations such as Eq. 1.5 to diagnose the output of climate models. A common value for the term $\frac{1}{4\sigma T^3}$ in Eq. 1.5 is 0.31 K/(W m^{-2}), which is related to the temperature at which Earth radiates to space (Bony et al. 2006). Substituting this numerical value for $\frac{1}{4\sigma T^3}$ into Eq. 1.5 leads to:

$$\Delta T = 0.31 \frac{\mathrm{K}}{\mathrm{W\,m^{-2}}} \Delta RF \tag{1.6}$$

We now examine the ***quantitative consistency*** between the rise in temperature (ΔT in Fig. 1.3) over the Anthropocene and the radiative forcing of climate attributed to humans (ΔRF in Fig. 1.3). The product $0.31\mathrm{K/W\,m^{-2}} \times 2.3\mathrm{W\,m^{-2}}$ is equal to 0.7 K (which is the same as 0.7 °C),[9] quite close to the observed rise in GMST (about 0.9 °C) over the course of the Anthropocene. As examined in detail in Chap. 2, the actual relationship between ΔT and ΔRF requires a consideration of factors such as climate feedback (i.e., enhancement or diminution of the RF of climate imposed by humans due to changes in factors such as atmospheric humidity and clouds) as well as the transport of heat from the atmosphere to the world's oceans, which specialists refer to as ocean heat export. It is likely, for instance, that positive feedback (enhancement) of the direct RF of climate caused by humans is

[9] Degrees Celsius and degrees Kelvin are identical when used to express temperature difference.

responsible for the difference between the expected (0.7 °C) and observed (0.9 °C) rise in GMST over the course of the Anthropocene. Most importantly, the calculation conducted above reveals ***quantitative consistency*** between the observed and expected rise in global temperature over the course of the Anthropocene. This is a critically important first step in the attribution of global warming to humans.

Several other aspects of global warming bear the human fingerprint. Climate models predict that as GHGs rise, the lowest layer of the atmosphere (the troposphere) will warm while the second layer of the atmosphere (the stratosphere) should cool. Stratospheric cooling is a consequence of the blanketing effect of GHGs: as atmospheric levels of GHGs rise, a larger fraction of the thermal energy emitted by the surface is absorbed, re-emitted, and therefore blocked from reaching the stratosphere. As shown in Fig. 1.5, tropospheric warming coupled with stratospheric cooling is seen in the climate record, at least over the part of the Anthropocene for which modern measurements of atmospheric temperature profiles exist (Sherwood and Nishant 2015). About two-thirds of the cooling of the upper stratosphere for the time period 1979–2005 has been attributed to rising GHGs, with the remainder attributed to human-induced depletion of stratospheric O_3 (Mitchell 2016). The pattern of temperature changes with respect to altitude and latitude throughout the troposphere and stratosphere agrees with the pattern predicted by climate models to a high degree of statistical significance (Santer et al. 2013a), although these models do tend to overestimate the amount of warming observed in the lower atmosphere (Santer et al. 2013b).[10]

Another important human fingerprint of global warming is the observation that the altitude of the tropopause, the boundary between the troposphere and the stratosphere, has been rising as predicted by climate models (Santer et al. 2013a). Had modern global warming been due to an increase in the luminosity of the Sun or a release of energy from the world's oceans, scientists would have expected to observe warming in the stratosphere and troposphere as well as little to no change in the height of the tropopause.

1.2.3.2 Carbon Dioxide

Carbon dioxide (CO_2) is the single greatest waste product of modern society. There is compelling scientific evidence that the rise in atmospheric CO_2 during the Anthropocene is due, nearly entirely, to human activity. The rise in CO_2 from 1765 to the early 1900s was predominately driven by the clearing of forests for agriculture (also known as land use change, or LUC) (Siegenthaler and Oeschger 1987). For a few decades subsequent to 1900, LUC and the combustion of fossil fuels made nearly equal contributions to the rise in atmospheric CO_2. Since the early 1950s, the growth of atmospheric CO_2 has been driven primarily by the combustion of fossil fuels[11] (Le Quéré et al. 2015).

[10] The tendency of many climate models to overestimate observed warming is a central theme of Chap. 2.

[11] Combustion of fossil fuels refers to the burning of coal, oil and gasoline, as well as natural gas (mainly methane) to meet society's needs for heat, electricity, transportation, and various other industrial enterprises.

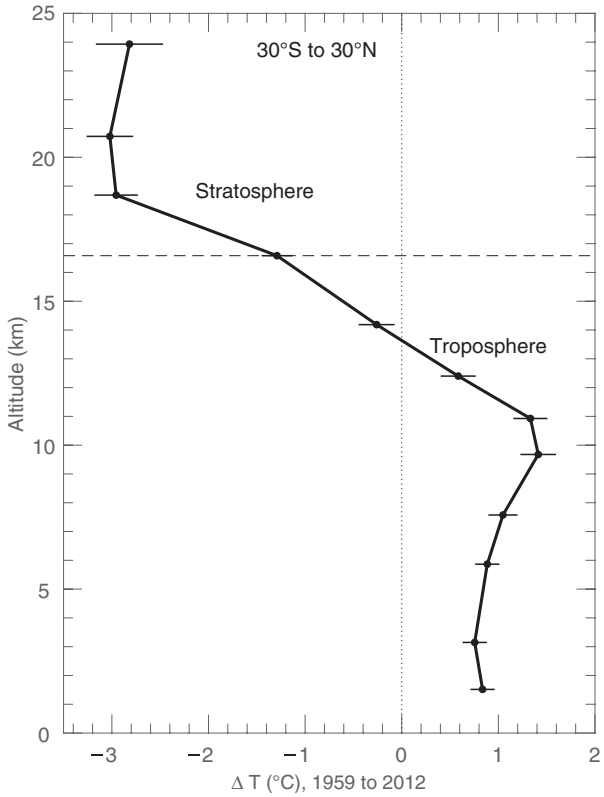

Fig. 1.5 Temperature change profile, 1959–2012. Temperature difference, 1959–2012, based on analysis of radiosonde observations acquired between latitudes of 30°S and 30°N (positive values indicate warming). After Sherwood and Nishant (2015) except we use altitude, rather than pressure, for the vertical coordinate. See Methods for further information

Precise quantification of the contemporary abundance of atmospheric CO_2 was initiated by Charles David Keeling at the Mauna Loa Observatory (MLO) in Hawaii during March 1958, as part of the International Geophysical Year (IGY) program (Keeling et al. 1976). On the first day of measurement, an atmospheric CO_2 abundance of 313 parts per million (ppm) was recorded.[12] The MLO CO_2 record is a signature accomplishment of the IGY, carried out from July 1957 to December 1958 and characterized by international cooperation on many scientific fronts. The ability of nations such as the United States and the Soviet Union to collaborate on IGY, despite the Cold War, serves as an inspiration for the level of international cooperation that will be needed to address the consequences of rising GHGs recorded at the Mauna Loa observatory.

On the day this sentence was written, atmospheric CO_2 at MLO was 407.66 ppm. This CO_2 reading amounts to a thirty percent increase relative to Keeling's first

[12] Mixing ratio denotes the fraction of all air molecules that exist as a particular compound. Keeling's initial observation means 313 out of every million air molecules were present as CO_2. The history of the Mauna Loa Observatory as well as an account of this initial observation are at https://scripps.ucsd.edu/programs/keelingcurve/2013/04/03/the-history-of-the-keeling-curve

observation and a forty-five percent increase relative to 280 ppm, the atmospheric mixing ratio of CO_2 commonly assumed to have been present at the start of the Anthropocene. Daily measurements of atmospheric CO_2 are provided at various websites, including https://www.co2.earth/daily-co2.

We now describe the scientific evidence that humans are responsible for the rise of CO_2. Our focus is on 1959 to present, the modern instrument era. Readers interested in learning about the human impact on CO_2 over the earlier part of the Anthropocene (i.e., prior to 1959) are encouraged to examine studies such as Siegenthaler and Oeschger (1987), Ruddiman (2003), Le Quéré et al. (2015), and Steffen et al. (2015).

Figure 1.6 shows time series of the atmospheric build-up of CO_2 and fossil fuel emissions of CO_2, from 1959 to present. Measurement of CO_2 at MLO (Keeling et al. 1976) and an estimate of global mean CO_2 provided by the US National Oceanographic and Atmospheric Administration (NOAA) Earth System Research Laboratory (ESRL) (Ballantyne et al. 2012) are shown in Fig. 1.6a. The saw-tooth pattern of the MLO CO_2 reveals the breathing of the biosphere: seasonal minimum occurs in late boreal summer just before deciduous trees, which predominantly exist in the NH, begin to drop their leaves. Seasonal maximum occurs in mid-spring of the NH, just before trees and plants bloom. The global, annual record of CO_2 exhibits a steady upward march over the past six decades.

Figure 1.6b provides our first evidence that humans are responsible for the rise of CO_2 over the past six decades. This panel compares the annual, global release of CO_2 to the atmosphere due to the combustion of fossil fuels (Boden et al. 2013) and land use change (Houghton et al. 2012) (green bars) to the annual rise in global atmospheric CO_2 (blue bars); both quantities are expressed in units of 10^9 metric tons of CO_2 (Gt CO_2) emitted per year.[13] In some years, such as 1977, 1979, 1987, 1988, and 1998, the rise in atmospheric CO_2 is more than half of the CO_2 input to the atmosphere by humans (i.e., the height of the blue bar is more than half the height of the green bar). Typically, the annual rise in the mass of atmospheric CO_2 (blue bars) equals between 40 and 50 % of the mass of CO_2 released to the atmosphere by humans (green bars). This comparison demonstrates ***quantitative plausibility*** that the observed rise in atmospheric CO_2 during the modern instrument era was indeed due to human activity.

Figure 1.7 illustrates the three most important pieces of observational evidence that scientists use to reveal the ***human fingerprint*** on rising CO_2. Time series of the mixing ratio of atmospheric CO_2 measured at MLO in Hawaii (19.82°N latitude) are compared to CO_2 measured at the South Pole Observatory (SPO) in Fig. 1.7a. Figure 1.8 compares the difference between annual averages of CO_2 at MLO and SPO ($\Delta CO_2^{MLO-SPO}$) for specific years plotted against the total human release of atmospheric CO_2 for each particular year. Figures 1.7a and 1.8 show that CO_2 is higher in the NH than the Southern Hemisphere (SH). This hemispheric gradient has long been used as evidence for the human influence on atmospheric CO_2, since anthropogenic emissions occur predominantly in the NH (Tans et al. 1990). The strong correlation of $\Delta CO_2^{MLO-SPO}$ versus total human release of CO_2 shown in

[13] CO_2 emissions are usually expressed as either Gt C or Gt CO_2. Here "G" stands for giga, the Greek word for giant, used as an abbreviation for a billion. Emissions in Gt C can be converted to Gt CO_2 by multiplying by 3.664 (Table 1 of Le Quéré et al. (2015)). Here and throughout, we use Gt CO_2 because these units are more convenient for evaluating the Paris Climate Agreement.

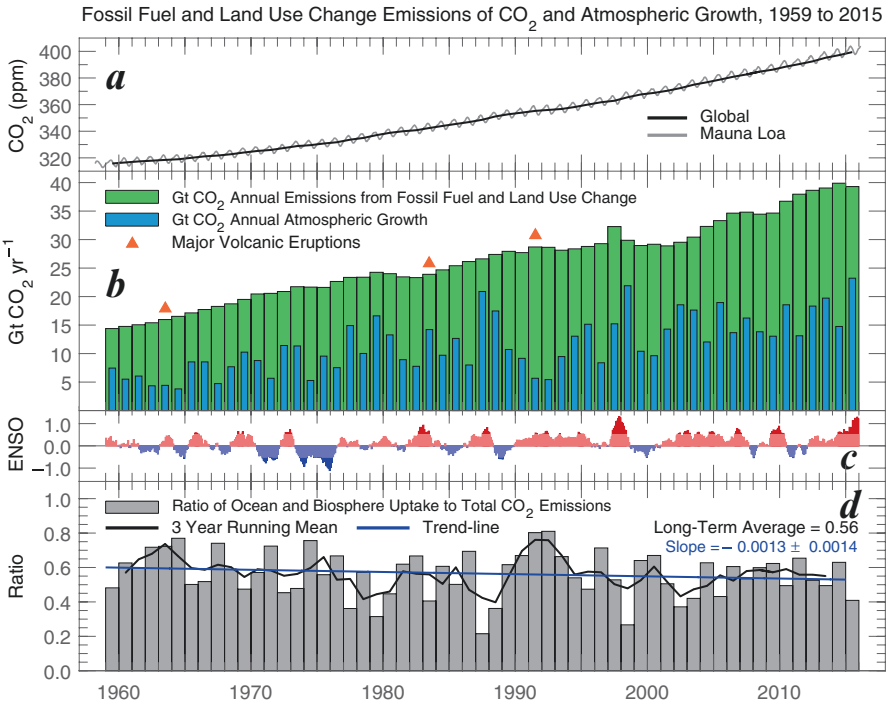

Fig. 1.6 Global carbon cycle, 1959 to present. (**a**) CO_2 mixing ratio from Mauna Loa Observatory (*grey*) (Keeling et al. 1976) and globally averaged CO_2 (*black*) (Ballantyne et al. 2012); (**b**) annual emissions of CO_2 to the atmosphere due to combustion of fossil fuels (Boden et al. 2013) and land use change (Houghton et al. 2012) in units of Gt CO_2 per year (*green bars*), growth of atmospheric CO_2 in the same units (*blue bars*) found from the rise in global annually averaged atmospheric CO_2, and the date of the eruptions of Mount Agung, El Chichón, and Mount Pinatubo (*orange triangles*); (**c**) monthly, Tropical Pacific ENSO Index (Zhang et al. 1997): periods of dark red longer than 5 months indicate an El Niño event; (**d**) ratio of ocean plus biospheric uptake of CO_2 divided by total emissions of CO_2 (i.e., difference between the height of the *green bar* and *blue bars* in panel (**b**) divided by the height of the *green bar*) (*grey*) as well as 3 year running mean (*black*) and trend-line of a linear least squares fit to the 3 year running mean (*blue*). See Methods for further information

Fig. 1.8 further demonstrates that the anthropogenic activity exerts primary control on the hemispheric gradient in atmospheric CO_2 (Fan et al. 1999).

Figure 1.7b illustrates the small decline of atmospheric O_2, which is another fingerprint of the human influence on rising CO_2 (see Methods for an explanation of the units and numbers). As CO_2 is released to the atmosphere by the combustion of fossil fuel, the oxygen (O) content of the newly emitted CO_2 comes from atmospheric molecular oxygen (O_2).[14] If rising atmospheric CO_2 were due to volcanic

[14] Fossil fuels are characterized by a mixture of hydrogen (H), carbon (C), and depending on the source other elements such as oxygen (O), nitrogen (N), and sulfur (S). Chemical compositions range from CH_4 (methane or natural gas), C_8H_{18} (octane, commonly used to represent automotive gasoline), to $C_{135}H_{96}O_9NS$ (coal, which can also contain other elements such as arsenic, lead, mercury, etc.). Since H and C are the dominant elements, fossil fuels are commonly called hydrocarbons. The O in CO_2 produced by combustion of methane or gasoline originates *entirely* from

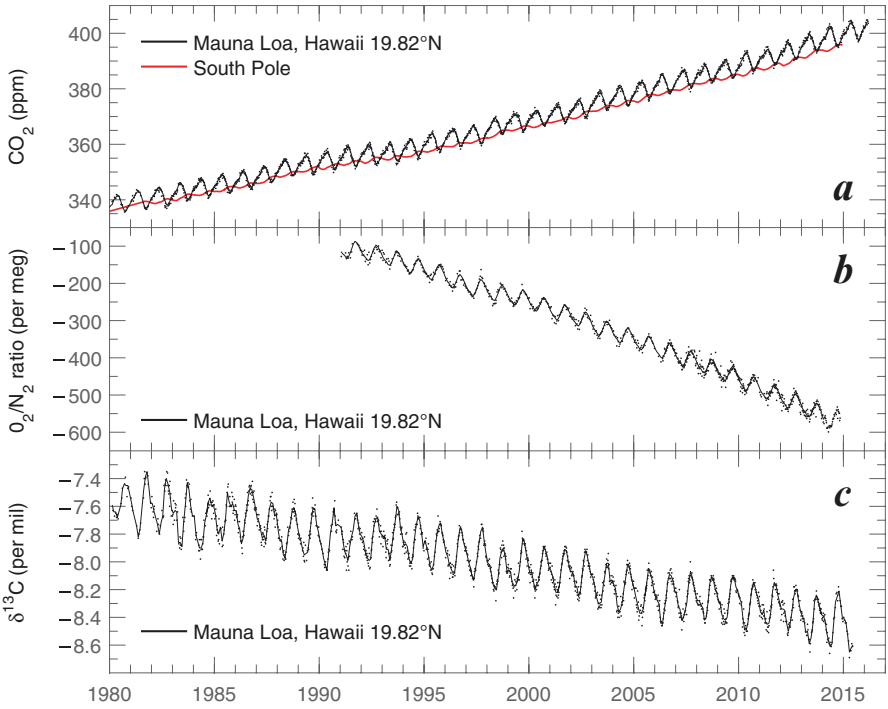

Fig. 1.7 Human fingerprint on rising CO_2. (**a**) Time series of CO_2 mixing ratio from Mauna Loa Observatory (*black*) (Keeling et al. 1976) and the South Pole (Tans et al. 1990); (**b**) ratio of atmospheric O_2 to N_2 measured at the Mauna Loa Observatory in units of per meg, where 1 per meg = 0.00001 % (Keeling et al. 1996); (**c**) abundance of ^{13}C in atmospheric CO_2 at Mauna Loa relative to a standard in units of per mil, where 1 per mil = 0.1 % (Keeling et al. 2005). See Methods for further information

activity or deep sea vents, atmospheric O_2 would be unaffected because the dominant form of outgassed carbon is CO_2, with the O drawn from abundant oxygen in Earth's crust. Measurement of atmospheric O_2 with sufficient precision to quantify the minute, putative decline was an instrumental challenge first overcome by Ralph Keeling (Keeling et al. 1996), the son of Charles David Keeling. The slight decline in atmospheric O_2 recorded in Fig. 1.7b provides strong quantitative evidence that combustion of fossil fuel is the driving factor behind rising CO_2.

The final human fingerprint involves the isotopic composition of atmospheric CO_2. The most common form of carbon has an atomic mass of 12 (^{12}C), due to the presence of six protons and six neutrons in the nucleus.[15] Carbon can exist in two other forms: carbon 13 (^{13}C) and carbon 14 (^{14}C), due to the presence of either 7 (^{13}C) or 8 (^{14}C) neutrons in the nucleus. The chemical properties of a compound are determined by the number of electrons, which equals the number of protons if a compound is neutral

atmospheric O_2, whereas the O in CO_2 produced by combustion of coal originates *mainly* from atmospheric O_2.

[15] Atomic mass is the sum of the number of protons and neutrons.

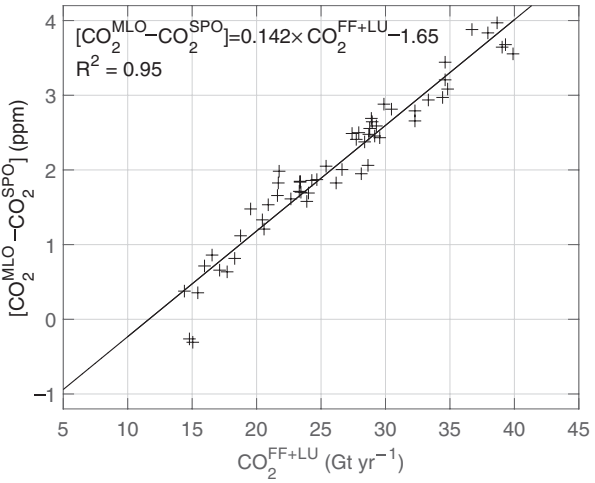

Fig. 1.8 Human fingerprint on hemispheric gradient of CO_2. Difference in annual average CO_2 at Mauna Loa Observatory (MLO) (Keeling et al. 1976) minus CO_2 at the South Pole Observatory (SPO) (Tans et al. 1990) (*vertical axis*) versus annual total emission of CO_2 to the atmosphere from the combustion of fossil fuels (Boden et al. 2013) and land use change (Houghton et al. 2012). Data span the time period 1959–2015. Numerical results of a linear least squares fit as well as the correlation coefficient are also given. See Methods for further information

(i.e., uncharged). Hence ^{12}C, ^{13}C, and ^{14}C are all considered to be different forms of carbon because they all contain six electrons. Most importantly, biological properties of a compound are mass dependent: our bodies prefer ^{12}C over the other two heavier forms of carbon that are digested, because lighter molecules diffuse more readily through our capillaries. The term isotopic composition, as used here, refers to the relative abundance of ^{13}C in a sample of atmospheric CO_2 compared to the sum of ^{12}C, ^{13}C, and ^{14}C in the same sample, and is expressed using the notation $\delta^{13}C$.

Figure 1.7c shows a time series of $\delta^{13}C$ recorded at MLO (Keeling et al. 2005). The downward decline of $\delta^{13}C$ means atmospheric CO_2 is getting isotopically lighter over time. In other words, at the start of the time series in 1980, the relative proportion of ^{13}C to ^{12}C in atmospheric CO_2 at Hawaii was larger than today. This serves as our final fingerprint because the carbon content of fossil fuels, which formed from the decomposition of plants on geologic time-scales, are isotopically light relative to contemporary atmospheric CO_2 (Whiticar 1996). If rising levels of atmospheric CO_2 during the time period shown in Fig. 1.7c had been due primarily to volcanoes, atmospheric CO_2 would have been expected to have gotten isotopically heavier (Rizzo et al. 2014), which is the opposite of what has been observed.

It is stated in Sect. 1.1 that over ***geologic time scales***, atmospheric CO_2 is controlled by volcanic activity and deep sea vents. Yet CO_2 shows no volcanic influence over the time of the modern instrument record. To further illustrate the lack of recent volcanic influence, the orange triangles in Fig. 1.6b have been placed at the time of eruption of Mount Agung, El Chichón, and Mount Pinatubo, the three largest eruptions over the past six decades. The growth of atmospheric CO_2 during the years of these eruptions (1963, 1982, and 1991) is unremarkable compared to other years: in fact, the growth of

atmospheric CO_2 (blue bars) after the eruption of Mt. Agung (1963) and Mt. Pinatubo (1991) is suppressed relative to prior years. The best estimate of contemporary release of atmospheric CO_2 by volcanoes and deep sea vents reveals release of about 0.26 Gt of atmospheric CO_2 per year (Marty and Tolstikhin 1998), less than 1 % of the human burden. Interestingly and with touching irony for those who refuse to accept the human influence on global warming, the volcanic release of CO_2 during the 9 h explosive phase of Mt. Pinatubo on 15 June 1991 likely matched the total, global release of CO_2 by humans ***on that day*** (Gerlach 2011). More than 20,000 days have passed since the start of modern measurements of atmospheric CO_2. On one day and one day only, global human release of atmospheric CO_2 was likely matched by a volcano. Human release of CO_2 has dwarfed volcanic release on the other 19,999 days.

Why have volcanoes been so dominant in the past, yet so unimportant in the present? One factor is that modern human civilization has not yet experienced a volcanic eruption of the magnitude known to have occurred in the past. The Volcanic Explosivity Index (VEI) denotes the size of volcanic eruptions (Newhall and Self 1982), much like the Richter Scale for earthquakes. Mt. Agung, El Chichón, and Mt. Pinatubo had VEIs of 5, 5, and 6, respectively. The most violent eruption Earth has experienced over the past 36 million years was the VEI of 9.1–9.2 eruption of La Garita[16] about 27.8 Mypb (Mason et al. 2004). Since the VEI scale is logarithmic with respect to volume of ejecta, a VEI 9 eruption would eject about 1000 times more mass than Mt. Pinatubo.[17] Had Mt. Pinatubo been VEI 9, it may have matched human emission of CO_2 over the prior 1000 days. In this case, of course, the ejection of CO_2 by such a monstrous event would have been the least of our concerns.

The other factor responsible for the minor role of volcanoes with respect to contemporary atmospheric CO_2 is that Earth is presently in a geologically dormant period. The Deccan Traps of India is one of the largest, most well-studied ancient volcanic features on Earth. Eruptions of this massive province, approximately 65 Mybp, may have been characterized by a decades-long explosive events (Self et al. 2006). The perturbation to atmospheric CO_2 by the Deccan Traps is the subject of active research, with some studies (Dessert et al. 2001) suggesting a considerably larger influence than others (Self et al. 2006).

We conclude by providing a brief overview of the latest understanding of the factors that control atmospheric CO_2. More detailed information, updated annually, is maintained at http://www.globalcarbonproject.org/carbonbudget.

It is well established that a substantial portion of the CO_2 released to the atmosphere by human activity is absorbed by trees and plants (i.e., the terrestrial biosphere) as well as the world's oceans (Le Quéré et al. 2015). Uptake of anthropogenic CO_2 by plants is facilitated by three factors: higher levels of atmospheric CO_2 promote faster growth of plants (Zhu et al. 2016), global warming has increased the length of the growing season (Le Quéré et al. 2015), and human supply of fixed nitrogen to the biosphere promotes a more fertile environment for plant growth (Galloway et al. 2014). The world's oceans

[16] The caldera of this ancient volcano is near the town of Creede, Colorado in the United States.

[17] For those with a mathematical background, the calculation is straightforward. The ejected mass is proportional to 10 raised to the power of VEI; therefore, the ratio of mass ejected by a VEI 9 eruption to Mount Pinatubo is 10^9 divided by 10^6, which equals 10^3 or 1000.

contain a mass of carbon about 50 times greater than that in the atmosphere and it has long been known that the world's oceans would uptake a portion of the CO_2 placed into the atmosphere by human activities (Revelle and Suess 1957).

An atmospheric and oceanic phenomena known as El Niño Southern Oscillation (ENSO) has been extensively studied as a driving factor for the variation of the height of the blue bars (atmospheric growth of CO_2) relative to the green bars (human release of CO_2) shown in Fig. 1.6b (Keeling et al. 2005; Randerson et al. 2005; Zeng et al. 2005). When the index shown in Fig. 1.6c is shaded dark red for a period of ~5 months or longer, the tropical ocean/atmosphere system is in the midst of an ENSO event.[18] The growth of atmospheric CO_2 tends to be larger than normal for about a year after the peak of an ENSO event, with the effect maximizing about 6 months after the peak (Zeng et al. 2005). An ENSO event affects atmospheric CO_2 due to suppression of oceanic uptake as well as the tendency for human-set fires to occur in drought stricken regions during certain ENSO years (Randerson et al. 2005). During late 2015, Earth experienced another major ENSO event, which likely was responsible for the more rapid rise of atmospheric CO_2 in 2015 compared to prior years. Indeed, the preliminary estimate of total human release of CO_2 in year 2015 given by Le Quéré et al. (2015), which is the origin of the last green bar in Fig. 1.6b, shows a slight decline relative to 2014. Should this decline in human release of CO_2 continue in future years, the height of the blue bars in future updates to Fig. 1.6b will fall relative to the value for 2015, except for years marked by either large ENSO events and/or extensive biomass burning.

The fraction of anthropogenic CO_2 removed each year via the world's terrestrial biosphere and oceans is depicted by the grey bars in Fig. 1.6d. There is considerable year-to-year variability, which has been widely studied and is attributed mainly to terrestrial biosphere (Bousquet et al. 2000; Le Quéré et al. 2003). Averaged over the entire data record, 56 % of the CO_2 released to the atmosphere by humans by the combustion of fossil fuels and land use change has been absorbed by land and ocean sinks. In other words, the actual rise in atmospheric CO_2 equals about 44 % of that known to have been emitted by humans.

The efficiency of the combined land and ocean sink for atmospheric CO_2 appears to be weakening over time. Figure 1.6d contains two lines. One shows a 3 year running mean (black) of the numerical values of each grey bar, for data starting in 1959 and ending in 2014. Values for 2015 are excluded from the 3 year running mean, because data for this year are considered preliminary at the time of writing. An entity such as a 3 year running mean is a common statistical method used to analyze data that exhibit a large amount of year-to-year variability, such as the grey bars in Fig. 1.6d. The trend-line (blue) shows a linear least squares fit to the 3 year running mean, another common technique used to examine geophysical data. The trend-line has a slope of −0.0013 per year, which means the fraction of anthropogenic CO_2 removed by the combined land and ocean sink may have declined from about 0.6 in 1959 to about 0.53 in 2014. However, there is considerable uncertainty (in this case,

[18] During an ENSO event warm waters in the Tropical Western Pacific ocean migrate to the Central and Eastern Pacific, causing shifts in the location of oceanic upwelling and atmospheric storms, as well as significant perturbations to the global carbon cycle. An informative animation of ENSO is provided at http://esminfo.prenhall.com/science/geoanimations/animations/26_NinoNina.html

±0.0014 per year) in the slope of the trend fit line. This uncertainty encompasses (albeit, just barely) the possibility that the combined land and ocean sink may not have actually changed and also, at the same time, another possibility that this uptake could have changed from 0.6 in 1959 to 0.45 in 2014. This analysis builds upon the work and supports the conclusions of Le Quéré (2010), who also emphasize the urgent need to reduce the uncertainty in the time rate of change of the combined land and ocean sink for human release of atmospheric CO_2. If the efficiency of the combined land and ocean sink for CO_2 is truly declining over time, then this is enormously important for the response of society to anthropogenic release of GHGs.

1.2.3.3 Methane

Methane (CH_4) is a vitally important anthropogenic GHG. The atmospheric abundance of CH_4 has risen from a pre-Anthropocene value of 0.7 ppm to a contemporary abundance of 1.84 ppm (Fig. 1.2). The rise in CH_4 between 1750 and 2011 has induced a RF of climate of 0.48 W m^{-2} (Fig. 1.4), second only to the RF of CO_2 among anthropogenic GHGs.[19] Methane is therefore commonly referred to as the second most important anthropogenic GHG.

Studies of atmospheric CH_4 are numerous, complex, and quite varied, owing to a variety of natural and human sources (see Kirschke et al. (2013) and references therein). Figure 1.9 shows an estimate of the sources (i.e., flux into the atmosphere) of CH_4, in units of 10^{12} g of CH_4 (Tg CH_4) emitted per year,[20] averaged over the decade 2000–2009 from Conrad (2009) and Kirschke et al. (2013). The figure also contains an estimate of the sinks (i.e., atmospheric loss) of CH_4 over the same period of time.

A number of scientifically important details regarding atmospheric CH_4 are contained in Fig. 1.9. First, the magnitude of the source is slightly larger than the sink, consistent with the fact that atmospheric CH_4 is rising. Also, there are various human and natural sources of considerable magnitude. As noted above, wetlands are the largest natural source of CH_4. Other natural sources include termites and the release of CH_4 from gas hydrates.[21] Finally, anthropogenic production of CH_4 occurs due to many aspects of our industrialized world, including the fossil fuel industry,

[19] The RF of climate due to CO_2 over the same time period was 1.82 W m^{-2}. The notion that CH_4 is a more potent GHG than CO_2 is reconciled with these two RF estimates upon realization that the rise of the atmospheric mixing ratio of CO_2 over the Anthropocene, 120 ppm, is about 106 times the rise of CH_4. For those who would like to dig into the numbers, radiative efficiencies of CO_2 and CH_4 are needed. In mixing ratio units, these radiative efficiencies are 1.4×10^{-2} W m^{-2} per ppm for CO_2 and 3.7×10^{-1} W m^{-2} per ppm for CH_4 (see Table TS.2 of IPCC (2007)). A "back of the envelope" estimate for the expected RF due to CH_4 is then:

$$[1.82 \text{ W m}^{-2} \times (3.7 \times 10^{-1} \div 1.4 \times 10^{-2})] \div 106 = 0.45 \text{ W m}^{-2} .$$

This estimate for the RF of CH_4 over the Anthropocene is quite close to the actual IPCC (2013) value of 0.48 W m^{-2}, which was found in a much more computationally intensive manner.

[20] Tera is derived from the Greek word teras, meaning monster, and is often used as a prefix to denote 10^{12}, or a trillion. A mass of 1 Tg (10^{12} g) is the same as one thousandth of a giga tonne, where tonne refers to metric ton.

[21] Methane hydrates are water ice structures that contains gaseous CH_4 in the core, and are prevalent in continental margins (Kvenvolden 1993).

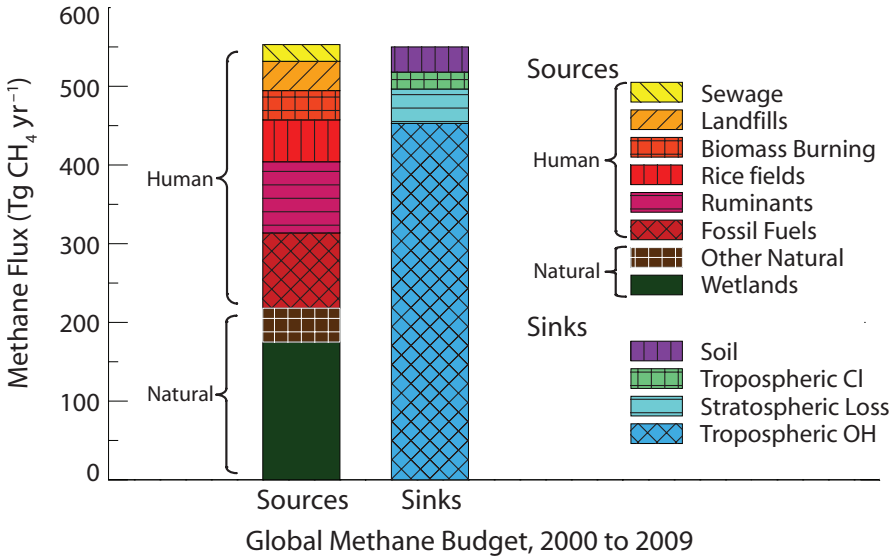

Fig. 1.9 Global methane budget. Source and sinks of atmospheric methane, over the decade 2000–2009, expressed as flux either into or out of the atmosphere. After Conrad (2009) and Kirschke et al. (2013). Human and natural sources, as well as components of all terms, are indicated. See Methods for further information

human set fires (biomass burning), microbial processes in the stomachs of ruminants,[22] as well as anaerobic conditions common in rice paddies and landfills. As detailed in Chap. 4, if human release of methane is to be curtailed, many aspects of modern society will need to be addressed, including how we heat our homes, generate our electricity, and produce our food.

Two considerable complications for the proper accounting of the human release of CH_4 are posed by possible alteration of the wetland source due to climate-change induced changes of the hydrologic cycle (i.e., floods and drought) as well as the possible release of prodigious amounts of CH_4 from the Arctic as permafrost thaws, due to global warming (Koven et al. 2011). For now, at least, the source of CH_4 due to Arctic permafrost is small on a global scale (Kirschke et al. 2013).

We turn our attention to the scientific importance of the numerical estimates of the CH_4 source and sink strengths shown in Fig. 1.9. The globally averaged sink for CH_4 is 550 Tg per year. The mass of CH_4 in the atmosphere, at present,[23] is about 5326 Tg. The atmospheric lifetime of CH_4 is given by:

[22] Ruminants are mammals such as cattle, sheep, deer, giraffes, etc. that acquire nutrients by fermenting plant-based foods in a specialized stomach prior to digestion.

[23] We can approximate the mass of CH_4 in the atmosphere by multiplying the mass of the entire atmosphere, 5.2×10^{21} g, by the mixing ratio of CH_4, which is 1.84 ppm or 1.84 out of every million air molecules. We must also account for the ratio of the atomic mass of CH_4 (16) to the mean atomic mass of air (28.8). The atmospheric mass of CH_4 therefore equals $1.84 \times 10^{-6} \times 5.2 \times 10^{21}$ g $\times (16/28.8) = 5.326 \times 10^{15}$ g $= 5326$ Tg.

$$\tau_{CH4} = \frac{Mass}{Removal\ Rate} = \frac{5326\text{Tg}}{550\text{Tg year}^{-1}} = 9.7\text{year} \tag{1.7}$$

On average, a molecule of CH_4 released to the atmosphere will persist for about a decade until it is removed by either a chemical reaction or a soil microbe. Prather et al. (2012) report a present-day CH_4 lifetime of 9.1 ± 0.9 years, consistent with our calculation above. Conversely, a lifetime of 12.4 years for CH_4 was used by IPCC (2013) in the calculation of GWPs because it is thought that the release of a large pulse of CH_4 to the atmosphere will prolong the atmospheric lifetime, due to resulting changes in the chemical composition of the tropical troposphere.

The ~10 year atmospheric lifetime for CH_4 has important policy implications. This is best illustrated by comparing the human release of CH_4 to that of CO_2. Throughout the world, humans presently release about 335 Tg of CH_4 and 39 Gt of CO_2 per year. Since 1000 Tg = 1 Gt, these sources are 0.335 Gt of CH_4 and 39 Gt of CO_2 per year: i.e., the mass of CO_2 released to the atmosphere each year by human society is about 116 times more than the mass of CH_4. The impact on climate is entirely dependent on the time scale of interest. Nearly all of the CH_4 released to the atmosphere in year 2015 will be gone by the end of this century. The ***CO_2-equivalent*** emission of CH_4, found by multiplying the current release by the GWP for CH_4 for a 100-year time horizon, is 28×0.335 Gt of CH_4 or 9.4 Gt per year. If our concern is global warming over the next century, then we would conclude the human release of CO_2 in year 2015 was about four times more harmful for climate ($39 \div 9.4 = 4.1$) than the release of CH_4. However, if our concern is the next two decades, we must consider the GWP of CH_4 over a 20-year time horizon. In this case, the CO_2-equivalent emission of CH_4 is 84×0.335 Gt or 28.1 Gt per year, and we would conclude the present human release of CH_4 is nearly as harmful for climate (28.1 versus 39) as the release of CO_2.

As noted above, international policy for the regulation of GHGs generally utilizes GWPs found over a 100-year time horizon. Perhaps this is appropriate, given CO_2 is such a long-lived GHG (i.e., a CO_2 molecule released today by humans will likely persist in the atmosphere longer than a molecule CH_4). However, should the world ever face an impending climate catastrophe in the midst of rapidly rising abundances of both atmospheric CO_2 and CH_4, the greatest leverage for near-immediate relief will be to reduce anthropogenic emissions of CH_4 (Shindell et al. 2009) or other short-lived pollutants (Pierrehumbert 2014). Of course this is much easier stated than accomplished given the wide variety of human activities that release CH_4, as well as the tendency for energy production in the United States to become increasingly more CH_4-based, given the abundant source of natural gas now being extracted by fracking.[24]

[24] The extraction of CH_4 by the hydraulic fracturing ("fracking") of ancient shale following horizontal drilling has led to a recent, major rise in production of this fossil fuel. This is discussed further in Chap. 4.

Considerable research effort has been directed towards quantification of the anthropogenic versus natural sources of atmospheric CH_4 due to the scientific importance of this apportionment. Suppose, as is likely, that CH_4 had the same (or nearly the same) lifetime for removal from the atmosphere as today, for conditions that prevailed prior to the Anthropocene. Also, if the natural source of atmospheric CH_4 was the same (or similar) for these two time periods, it can be shown that:

$$\frac{CH_4^{\text{Pre-Anthropocene}}}{CH_4^{\text{Present}}} = \frac{Source^{\text{Natural}}}{Source^{\text{Natural+Human}}} \tag{1.8}$$

where $Source^{\text{Natural}}$ is the present natural flux of CH_4 to the atmosphere and $Source^{\text{Natural+Human}}$ is the total flux. Using the numerical values for these two fluxes[25] from Fig. 1.9, which are based on Table 1 of Kirschke et al. (2013), yields an estimate for $CH_4^{\text{Pre-Anthropocene}}/CH_4^{\text{Present}}$ of 0.39. This estimate is astonishingly close to the actual ratio of $CH_4^{\text{Pre-Anthropocene}}/CH_4^{\text{Present}} = 0.38$, found using the atmospheric abundances given in the opening paragraph of this section.[26] Thus, an analysis of the sources of atmospheric CH_4 for the contemporary atmosphere provides ***strong quantitative support*** for the notion that human activities are indeed responsible for the rise of atmospheric CH_4 over the course of the Anthropocene.

1.2.3.4 Nitrous Oxide, Ozone, and Ozone Depleting Substances

Nitrous oxide (N_2O) is commonly considered to be the third most important anthropogenic GHG. The atmospheric abundance of N_2O has risen from a pre-Anthropocene value of 0.273 ppm to a contemporary abundance of 0.329 ppm (Fig. 1.2). The rise in N_2O between 1750 and 2011 has induced a RF of climate of 0.17 W m^{-2} (Fig. 1.4).

Nitrous oxide is long-lived, with a lifetime of about 120 years. The vast majority of the atmospheric loss of N_2O occurs in the stratosphere (Minschwaner et al. 1993). Nitrous oxide has a GWP of 264 (20-year time horizon) or 265 (100-year time horizon) (Table 1.1) according to IPCC (2013). The GWP of N_2O is nearly the same for both time horizons because a pulse of N_2O released to the atmosphere decays, within models used to calculate GWPs, in a manner quite similar to the decay of a pulse of CO_2.

Current best understanding of the human sources of N_2O is described in Chap. 6 of IPCC (2013). The total anthropogenic source is estimated to be 21.7 Tg of N_2O per year,[27] albeit with considerable uncertainty. The human source could be as low

[25] $Source^{\text{Natural}} = 218$ Tg $year^{-1}$ (total of the human terms; i.e., height of the six rectangles to the right of "Human" in Fig 1.9); $Source^{\text{Natural+Human}} = 553$ Tg $year^{-1}$ (total of all sources, Fig. 1.9).

[26] These abundances yield $CH_4^{\text{Pre-Anthropocene}}/CH_4^{\text{Present}} = 0.7$ ppm/1.84 ppm = 0.38.

[27] The IPCC (2013) best estimate for human release of N_2O is 6.9 Tg of nitrogen per year, but we must convert to N_2O to make use of the GWP of N_2O. 6.9 Tg of N per year is the same as $6.9 \times (44 \div 14) = 21.7$ Tg of N_2O per year, where 44 and 14 are the atomic masses of N_2O and N.

as 8.5 or as high as 34.9 Tg N_2O per year according to Table 6.9 of IPCC (2013). Prather et al. (2012) report a smaller best estimate for the human source of 20.4 Tg N_2O per year, with a reduced uncertainty of ±4 Tg N_2O per year. Agriculture is the dominant activity responsible for human release of N_2O: use of nitrogen fertilizers results in release of N_2O to the atmosphere due to microbial processes in soils (Smith et al. 1997). Contemporary human emissions of N_2O presently make a contribution to global warming[28] that is ~15 % that of emissions of CO_2.

The largest natural sources of N_2O are production from soils that lie beneath vegetation unperturbed by humans and release from the world's oceans. The natural source is estimated to be 34.6 Tg of N_2O per year, again with considerable uncertainty (range from 17.0 to 61.6 Tg of N_2O per year) (IPCC 2013). Large uncertainties for both the human and natural sources of N_2O, as well as the long atmospheric lifetime for N_2O, preclude meaningful use of Eq. 1.8 to examine the consistency between the rise in N_2O and our understanding of the natural and anthropogenic source strengths. Nonetheless, the long-term rise in N_2O since 1977, the observation of larger abundances in the NH than the SH documented on websites such as http://www.esrl.noaa.gov/gmd/hats/combined/N2O, and field measurements of strong anthropogenic sources (Table 6.9 of IPCC (2013)) all provide strong scientific evidence that humans are responsible for the vast majority of the rise in N_2O over the course of the Anthropocene.

The possible increase in atmospheric N_2O due to expanded use of biofuels will receive considerable attention in the next few decades. There is considerable interest in the development of biofuels as a replacement for fossil fuels because, in theory, biofuels could be close to carbon neutral. The notion of carbon neutrality is predicated on the fact that the carbon in a hydrocarbon fuel produced by recent photosynthesis has been drawn out of the atmosphere just prior to combustion: i.e., the carbon is recycled. One of the many concerns regarding the modern biofuel industry is that the associated increase in production of atmospheric N_2O due to the need for additional fertilizer will offset the climate benefit from the supposed carbon neutrality of this new fuel source (Crutzen et al. 2016).

The effect of N_2O on stratospheric O_3 will also likely receive attention by researchers. Loss of N_2O occurs in the stratosphere and, upon decomposition, N_2O produces compounds that deplete stratospheric ozone (Ravishankara et al. 2009). Most interestingly, the ozone depletion potential[29] of N_2O depends on future atmospheric abundances of CO_2 and CH_4 (Revell et al. 2015). Not only are CO_2, CH_4, and N_2O (as well as chlorofluorocarbons, or CFCs) all important for climate, but these compounds are also inextricably linked for the future recovery of Earth's ozone layer.

[28] Recalling that 1000 Tg = 1 Gt, the human release of CO_2 is 39 Gt C per year, and making use of a GWP for N_2O of 264 results in the following calculation for the contribution of N_2O to global warming relative to that of CO_2: $[21.7\ \text{Tg year}^{-1} \div 1000\ \text{Tg/Gt}] \div [39\ \text{Gt year}^{-1}] \times 264 = 0.15$.

[29] Ozone depletion potential is a metric developed by atmospheric chemists to gauge the harmful effects of various compounds on the stratospheric ozone layer.

While it is certainly true that most scientists consider N_2O to be the third most important anthropogenic GHG, it is worth noting that the contribution to the RF of climate over the course of the Anthropocene by N_2O is smaller than that of both Ozone Depleting Substances (ODS) and tropospheric O_3 (Fig. 1.4). Why then is N_2O commonly considered to be the third most important anthropogenic GHG? The answer is nuanced but provides insight into the multi-disciplinary nature of modern atmospheric science.

The category labeled ODS in Fig. 1.4 consists of many gases (see Methods), including numerous CFCs, hydrochlorofluorocarbons (HCFCs), carbon tetrachloride (CCl_4), methyl chloroform (CH_3CCl_3), etc. Industrial production of this class of compounds has been successfully regulated by the Montreal Protocol and subsequent amendments due to the harmful effects of these chemicals on Earth's protective ozone layer (WMO 2014). It is not commonly appreciated, but the climate protection accomplished by the Montreal Protocol (due to reduction in the atmospheric abundance of ODS that would have otherwise occurred) far exceeds the climate protection accomplished by the Kyoto Protocol (Velders et al. 2007). In other words, the positive RF of climate due to ODS in Fig. 1.4 would have been much larger had industrial production of these compounds not been halted by the Montreal Protocol. Nonetheless, most scientists do not apply the GHG label to the class of chemical compounds that deplete Earth's ozone layer. Also, none of the ODS compounds, alone, has a RF of climate as large as N_2O. So N_2O survives this challenge to its third place status.

The category labeled tropospheric O_3 in Fig. 1.4 also exerts a RF of climate that exceeds that due to N_2O. Over the course of the Anthropocene, human release of chemicals such as carbon monoxide and nitrogen oxides produced by biomass burning and the combustion of fossil fuels has led to a build-up of tropospheric ozone, exerting a considerable influence on the RF of climate (Fig. 1.4). There has also been a slight cooling effect to the decline in stratospheric O_3 over the Anthropocene. Lack of consideration of tropospheric O_3 as the third most important anthropogenic GHG is due to various factors, including: (a) tropospheric O_3 is not emitted directly by humans but rather is produced in the atmosphere following chemical reactions of O_3 precursors released by humans; (b) surface O_3, which is an important subcategory of tropospheric O_3, is regulated by air quality agencies throughout the world (i.e., O_3 poses more harm to air quality than to climate); (c) all of the other anthropogenic GHGs tend to be long lived (atmospheric lifetimes greater than a year) and have nearly uniform global distributions, whereas tropospheric O_3 is short lived (atmospheric lifetime of minutes to hours) and is highly variable. In the minds of most climate scientists, N_2O survives the challenge from tropospheric O_3 to its third place ranking among anthropogenic GHGs.

We conclude this section by noting the radiative forcing of climate due to tropospheric ozone is due mainly to enhancements over background levels in the tropical upper troposphere (Shindell and Faluvegi 2009). Elevated levels of ozone in this region of the atmosphere are mainly due to biomass burning (Anderson et al. 2016). It is therefore likely that air quality regulations in the developed world will have little effect on the RF of climate due to tropospheric O_3, since so much of the developed

world is outside of the tropics. Reducing human set fires in the tropics is a vexing problem, given that many of the fires are set to clear land for agriculture. Nonetheless, the development of effective controls on human set fires will likely be necessary to reduce the RF of climate due to tropospheric O_3 (Keywood et al. 2013).

1.2.3.5 HFCs, PFCs, SF_6 and NF_3

Sulfur hexafluoride (SF_6) and the class of compounds called hydrofluorocarbons (HFCs) and perfluorocarbons (PFCs) often appear in the climate regulation lexicon because these compounds, along with CO_2, CH_4, and N_2O, were all considered by the original Kyoto Protocol. Over the course of the Anthropocene, it is estimated that the RF of climate due to SF_6, HFCs, and PFCs has been about 0.03 W m^{-2} (Other F-gases, Fig. 1.4), which is about 1 % of the total RF of climate due to all anthropogenic GHGs. Nonetheless, there is concern the RF of climate of these compounds could rise in the future (IPCC/TEAP 2005; Velders et al. 2009; Zhang et al. 2011). The Doha amendment, adopted in December 2012, added nitrogen trifluoride (NF_3) to the list of GHGs in the Kyoto Protocol. As such, we'll provide a brief description of the lifetimes, GWP, and industrial uses of HFCs, PFCs, SF_6, and NF_3.

First a little demystification of the chemistry. All of the compounds considered in this section contain at least one fluorine (F) atom, which is in the halogen column of the periodic table. Also and most importantly, none of the compounds discussed here contain any chlorine or bromine atoms. Chlorine (Cl) and bromine (Br), two other halogens, are harmful to Earth's ozone layer and any industrial compound containing either Cl or Br that has a long enough lifetime to reach the stratosphere falls under the auspices of the Montreal Protocol. Natural production of HFCs, PFCs, SF_6 and NF_3 does not occur. Therefore, the presence of these compounds in the atmosphere at a detectable level is attributed to human activity.

The HFCs, PFCs, SF_6 and NF_3 group of GHGs are chemically stable and radiatively active. Most of these compounds have either a single central element surrounded by either numerous fluorine atoms or some combination of fluorine and hydrogen atoms, or a central double carbon similarly surrounded. These chemicals have various physical properties that have resulted in a wide range of industrial applications. The molecular structure of these compounds makes them very long lived: most survive intact until they encounter the intense ultraviolet radiation environment of Earth's upper stratosphere, except for some HFCs that are removed by chemical reactions in Earth's troposphere. Finally, the presence of F in these molecules creates what scientists call a strong dipole moment. These dipole moments tend to occur at wavelengths where thermal radiation emitted by Earth's surface would otherwise escape to space (i.e., an atmospheric window). Chemicals that are long-lived and absorb in an atmospheric window tend to have large GWPs. Typically, the more F in a compound, the higher the GWP (Bera et al. 2009).

Table 1.2 gives the GWPs (100-year time horizon), atmospheric lifetimes, and industrial uses of HFCs, PFCs, SF_6, and NF_3. The information is based on Table 8.A.1 of IPCC (2013) and is intended to serve as a synopsis of this longer table, which

Table 1.2 Properties of long lived HFCs, PFCs, SF_6, and NF_3

GHG	GWP[a]	Lifetime (years)	Industrial use
HFCs	116–12,400	1.3–242	Refrigeration, foam blowing, and by product of manufacturing of HCFCs
PFCs	6290–11,100	2000–50,000	Aluminum smelting
			Semi-conductor manufacturing
SF_6	23,500	3200	Insulator in high voltage electrical equipment
			Magnesium casting
			Semi-conductor manufacturing
NF_3	16,100	500	Semi-conductor manufacturing

[a]For 100-year time horizon

spans four pages, covers more than 100 compounds, and contains many properties for each compound. Only ranges of GWPs and lifetimes are given for HFCs and PFCs in Table 1.2. The atmospheric lifetime for some of these molecules is remarkably long (CF_4, a PFC, has a lifetime of 50,000 years) and many of the GWPs are huge (C_2F_6, another PFC, has a GWP of 11,100).

Hydrofluorocarbons (HFCs) reside at the intersection of ozone depletion and global warming. The Montreal Protocol, which was enacted to protect Earth's ozone layer, guided a transition from industrial production of CFCs to a class of gases called hydrochlorofluorcarbons (HCFCs), because HCFCs are less harmful to the O_3 layer than CFCs.[30] The Montreal Protocol requires a further transition from HCFCs to hydrofluorcarbons (HFCs) because, as noted above, HFCs pose no threat to the ozone layer. However, the GWPs of HFCs (Table 1.2) generally far exceed the GWPs of HCFCs (Table 8.A.1, IPCC (2013).

The future RF of climate due to HFCs is uncertain. Velders et al. (2009) project the RF of climate due to HFCs could be 0.4 W m^{-2} by mid-century, considerably larger than the RF due to HFCs considered by IPCC (2013). The primary reason for this difference is their projection of considerably larger growth in the atmospheric abundance of HFC-125 (formula CHF_2CF_3; lifetime = 28 years; GWP = 3170) than in the scenarios used to guide the IPCC climate models.

A number of scientists and policy-makers have lobbied for HFCs to be removed from the UNFCCC basket of GHGs and placed under the auspices of the Montreal Protocol. The argument for this transition is twofold: (1) the production of HFCs was initiated by the Montreal Protocol; (2) this governing body has been extraordinarily effective due to close cooperation between atmospheric scientists, the chemical manufacturing industry, and policy members who staff the Parties of the

[30] CFCs are a class of chemicals that contain chlorine, fluorine, and carbon atoms, whereas HCFCs are a class of chemicals that contain hydrogen, chlorine, fluorine, and carbon atoms. In some ways, bookkeeping would be easier had the former been labeled ClFCs and the latter HClFCs. Alas, the first "C" in these compounds stands for chlorine and the second stands for carbon. To make matters more confusing, HFCs are chemicals that contain only hydrogen, fluorine, and carbon atoms. Here the "C" stands for carbon. So if the C comes after the F, it stands for carbon.

Montreal Protocol. Also, it is worth noting that it is inconceivable that the gross domestic product of any country could be adversely affected by regulation of HFCs. In other words, the stakes for the world's economies are low with regard to regulation of HFCs. On 15 October 2016, at the 28th Meeting of the Parties of the Montreal Protocol held in Kigali, Rwanda, an agreement was reached to regulate the future production of HFCs under the Montreal Protocol. This marks the first time the Montreal Protocol has had direct authority over a class of chemical compounds that pose no threat to the ozone layer.

Perfluorocarbons (PFCs) are a class of compounds containing only carbon and fluorine that resist heat, oils, and staining. The most abundant PFCs are PFC-14 (CF_4), PFC-116 (C_2F_6), and PFC-218 (C_3F_8). Atmospheric levels of these compounds have risen steadily; contemporary levels of CF_4, C_2F_6, and C_3F_8 are a factor of 2, 4, and 10 larger, respectively, than observed during the onset of observations in the early 1970s (Mühle et al. 2010). It has been projected that the RF of climate due to all PFCs could approach 0.04 W m^{-2} by end of this century (IPCC/TEAP 2005; Zhang et al. 2011). While this would represent only a small contribution to global warming, PFCs will continue to be monitored due to their extremely long atmospheric lifetimes (Table 1.2).

Sulfur hexafluoride (SF_6) is an excellent insulator favored in the high voltage, electric industry because this compound is non-flammable.[31] The atmospheric abundance of SF_6 has risen steadily since the early 1970s and shows no sign of abating (Rigby et al. 2010). It has been estimated that the RF of climate due to SF_6 could reach 0.037 W m^{-2} by the end of the century (Zhang et al. 2011). As for PFCs, SF_6 bears monitoring due to its atmospheric lifetime of 3200 years (Table 1.2).

The sulfur and fluorine compound sulfuryl fluoride (SO_2F_2) is used as an insecticide and is also monitored, due to a GWP of 800. However, SO_2F_2 has a lifetime of only 36 years. As a result, atmospheric abundances would decline relatively soon after any corrective action were taken, if such action were ever needed.

The sulfur, fluorine, and carbon containing compound SF_5CF_3 received considerable attention in the media following discovery of a surprisingly large atmospheric abundance (Sturges et al. 2000). This gas was termed a "super GHG" because it has the highest radiative efficiency, 0.57 W m^{-2} ppb^{-1}, of any GHG ever studied. However, recent measurements reveal a slowdown in the emissions to the atmosphere (Sturges et al. 2012) and the present RF of climate of SF_5CF_3 is a miniscule ~8.6×10^{-5} W m^{-2}.[32]

Finally, nitrogen trifluoride (NF_3) is the latest member of the GHG-club. In 2008, several studies appeared calling attention to the RF of climate due to this previously unappreciated compound (Prather and Hsu 2008; Tsai 2008). As noted above, NF_3 was added to the Kyoto Protocol list of GHGs as part of the Doha amendment in 2012. The lifetime and GWP of NF_3 are given in Table 1.2. The primary atmo-

[31] At one time SF_6 was used to cushion sports shoes, but this use ceased a decade ago and is not considered to be atmospherically important.

[32] Atmospheric abundance of SF_5CF_3 was 0.00015 ppb in 2012 (Sturges et al. 2012); RF of SF_5CF_3 = 0.00015 ppb × 0.57 W m^{-2} ppb^{-1} = 8.6×10^{-5} W m^{-2}.

spheric release of NF_3 seems to be due to the manufacture of large, liquid crystal display screens (Thomas et al. 2012). The present RF of climate due to NF_3 is small, $\sim 2.4 \times 10^{-4}$ W m^{-2}.[33] Perhaps this late-comer to the GHG-club will one day be known as the couch potato GHG.

1.2.3.6 Aerosols

Aerosols are small solid or liquid particles suspended in air. In the context of this book, we use aerosols to refer to particles either emitted directly into the atmosphere by a particular human activity (typically fossil fuel combustion or fires) or particles that form following chemical and physical transformations in the atmosphere of pollutants known as aerosol precursors. The only natural aerosols we shall consider are those resulting from volcanic eruptions; volcanic aerosols only affect climate if they exist in the stratosphere.

Aerosols, particularly those containing the element sulfur, reflect incoming solar radiation, which cools the surface. Sulfate aerosols tend to be produced from pollutants emitted by coal-fired power plants, ships, and diesel fueled trucks and cars, although there is a strong movement towards use of ultra-low sulfur diesel fuel in some parts of the world (Krotkov et al. 2016). Volcanic aerosols, which exert short-term climatic cooling, are also composed of sulfate (Lacis and Mischenko 1995). Sooty aerosols, termed black carbon, are likewise produced by combustion of fossil fuels and biomass burning. Black carbon aerosols have a warming effect because these particles absorb solar radiation (Bond et al. 2013).

The association of human activity with the presence of tropospheric aerosols is well established from both ground-based (Jimenez et al. 2009; Yoon et al. 2016) and space-based observations (Streets et al. 2013; Yoon et al. 2014; He et al. 2016; McLinden et al. 2016). Yet, quantification of the RF of climate due to tropospheric aerosols continues to pose a scientific challenge due to the inability to precisely define numerical values of both the direct modulation of RF by anthropogenic aerosols (Myhre 2009; Kahn 2012; Bond et al. 2013) and the changes in RF driven by the effect of aerosols on clouds (Morgan et al. 2006; Carslaw et al. 2013). The IPCC (2013) best estimate and uncertainty of ΔRF over the course of the Anthropocene for these two terms, labeled Aerosol Direct Effect and Aerosol-Cloud Interaction, are shown in Fig. 1.4.

Tropospheric aerosols lie at the nexus of public health, air quality, and climate change. Exposure to small (Dominici et al. 2006) and/or toxic (Bell et al. 2007) aerosols has deleterious effects on human health. As a consequence, movements are underway throughout the world to reduce both the direct emission of aerosols as well as the emission of aerosol precursors. Reductions in the abundance of tropospheric aerosols and aerosol precursors, in response to air quality legislation motivated by public health concerns, have been readily observed by space-borne

[33] Atmospheric abundance of NF_3 peaked at 0.0012 ppb in late 2011 (Arnold et al. 2012) and radiative efficiency is 0.2 W m^{-2} ppb^{-1} (Table 8.A.1 of IPCC (2013); RF of NF_3 = 0.0012 ppb $\times$ 0.2 W m^{-2} ppb^{-1} = 2.4×10^{-4} W m^{-2}.

instrumentation throughout the world (Streets et al. 2013; Yoon et al. 2014; He et al. 2016). As such, the climate system is presently transitioning from an era where the cooling of climate due to aerosols may have had close to comparable strength as GHG induced warming to an era where the radiative warming due to GHGs will dominate aerosol cooling (Smith and Bond 2014).

The transition to a GHG dominated regime is illustrated in Fig. 1.10. This figure shows ΔRF due to CO_2, CH_4, and N_2O as well as all anthropogenic GHGs from 1850 to 2100 for the Representative Concentration Pathway (RCP) 4.5 scenario (Thomson et al. 2011) used throughout IPCC (2013). Total ΔRF due to all anthropogenic GHGs reaches 4.5 W m^{-2} in year 2100, as designed. The error bars for the ΔRF terms of GHGs, placed at year 2011, are from IPCC (2013). These uncertainties represent 5 and 95 % confidence intervals.

Figure 1.10 shows 71 plausible values for time series of ΔRF due to tropospheric aerosols published by Smith and Bond (2014). The colors correspond to least cooling (reds) to most cooling (blues); the black line denotes the central (median) scenario. These estimates are based on time series of the direct RF of climate due to black carbon, organic carbon, and sulfate aerosols as well as the effect of aerosols on clouds, all tied to the emissions of aerosols and aerosol precursors from the RCP 4.5 scenario. There exists considerable uncertainty with each of these terms. Most importantly, these uncertainties are handled in a self-consistent manner for each of the 71 scenarios over the time period 1850–2100. The scenarios colored in red (least cooling) assume black carbon aerosols exert considerable warming of climate, offsetting nearly all of the cooling by sulfate and organic carbon and the effect of aerosols of clouds. Conversely, the scenarios colored in blue (most cooling) assume black carbon aerosols exert little warming and that sulfate plus organic carbon, combined with the cloud response have led to about 1.4 W m^{-2} cooling in year 2011. For these large cooling scenarios, tropospheric aerosols offset nearly half of the ~2.8 W m^{-2} warming due to GHGs in year 2011.

The difference between the blue and red curves represents the uncertainty in the radiative forcing of climate due to aerosols. As we shall see in Chap. 2, this uncertainty limits our ability to forecast future global warming. All of the aerosol scenarios converge to near zero ΔRF in year 2100. Forecast values of ΔT in 2100 depend on ΔRF from GHGs (known well, provided CO_2, CH_4, N_2O, and the minor GHGs are specified) combined with the true value of climate feedback (see Sect. 2.2.1.2). The climate record over 1850 to present can be fit nearly equally well under two contrasting scenarios: (i) the true value of aerosol RF happened to be little cooling (red curves, aerosols, Fig. 1.10) in which case climate feedback must be modest; (ii) the true value of aerosol RF happened to be large cooling (blue curves) in which case climate feedback must be considerable. If we assume the feedback inferred from the climate record persists over time, then the future rise in ΔT for the modest feedback scenario will be considerably smaller than the future rise in ΔT for the considerable feedback scenario. Even though the human fingerprint on tropospheric aerosol loading is extremely well established, uncertainty in the climatically critical quantity ΔRF due to aerosols leads to considerable spread in future projections of global warming.

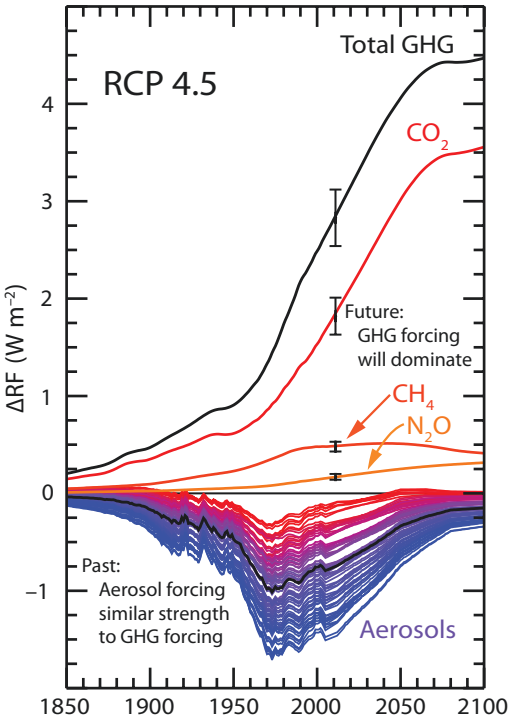

Fig. 1.10 The rise and fall of RF due to aerosols. Time series of radiative forcing of climate (ΔRF) due to CO_2, CH_4, N_2O, and all anthropogenic GHGs, from 1850 to 2100, based on the RCP 4.5 scenario (Meinshausen et al. 2011) (*top*) and 71 plausible scenarios for total ΔRF due to anthropogenic aerosols (combination of the aerosol direct effect and the aerosol-cloud interaction) from Smith and Bond (2014) (*bottom*). See Methods for further information

1.3 Methods

Most of the figures are composites formed by combining data from publicly available data archives. Here we provide details on webpage addresses of these archives, citations to the scientific papers that describe the measurements, as well as details regarding how the data has been processed. Electronic copies of the figures are available on-line at http://parisbeaconofhope.org.

Figure 1.1 shows estimates of the global mean surface temperature anomaly (ΔT) relative to the pre-industrial baseline and the mixing ratio of atmospheric CO_2, plotted using a logarithmic scale. The figure is broken up into six intervals, denoted using Era. Sources of ΔT and CO_2 for each Era are described below.

Era 1, **ΔT** is based on two data records:

(i) 1850 to present: the HadCRUT4.4.0.0 global, annual mean temperature record based on thermometer measurements, provided by the Climatic Research Unit (CRU) of the University of East Anglia, in conjunction with the Hadley Centre of the United Kingdom Met Office (Jones et al. 2012), archived at:
http://www.metoffice.gov.uk/hadobs/hadcrut4/data/4.4.0.0/time_series/HadCRUT.4.4.0.0.annual_ns_avg.txt
Column 2 of this file tabulates ΔT relative to their 1961–1990 baseline. We have added 0.3134 °C to each data point, in order to place the measurements on the

1850–1900 baseline used throughout this book (i.e., the mean value of ΔT after this adjustment, averaged over years 1850–1900, is by definition zero).

(ii) 1000 ybp to 1849: a temperature reconstruction based on various proxies, such as tree rings, corals, etc. published by Jones and Mann (2004), archived by the National Centers for Environmental Information (NCEI) of the US National Oceanographic and Atmospheric Administration (NOAA) at:
ftp://ftp.ncdc.noaa.gov/pub/data/paleo/contributions_by_author/jones2004/jonesmannrogfig5.txt
Column 6 of this file tabulates global ΔT smoothed with a low pass filter, relative to their 1856–1980 baseline; 0.2657 °C has been added to place the measurements on our 1850–1900 baseline.

Eras 2 and 3, **ΔT** is based on the European Project for Ice Coring in Antarctica (EPICA) Dome C record (Jouzel et al. 2007) archived at:

http://www1.ncdc.noaa.gov/pub/data/paleo/icecore/antarctica/epica_domec/edc3deuttemp2007.txt

This record is based on analysis of the isotopic composition of the ice core, which is sensitive to temperature conditions at the time the ice formed. Two adjustments have been applied. First, we have subtracted 0.4250 °C from each data point to place the record on our 1850–1900 baseline. Second, since the ice core record represents temperature anomalies in Antarctica, which are larger than for other parts of the world, we have multiplied each data point by 0.463 to account for this difference. This multiplicative factor, based on analysis of the relation between Arctic and global warming over the modern time period (Chylek and Lohmann 2005), is in good agreement with the climate model simulations of the relation between warming in Antarctica and throughout the world (Masson-Delmotte et al. 2006).

Eras 4 and 5, **ΔT** is based on changes in Earth's surface temperature inferred from observations of isotopic composition of the shells preserved in deep seas cores (Hansen et al. 2013), archived at Columbia University:

http://www.columbia.edu/~mhs119/Sensitivity+SL+CO2/Table.txt

Data in column 6, labeled Ts, are used. The authors have related these deep sea core inferences to 14 °C, which is the globally averaged surface temperature from 1961 to 1990. We have subtracted 14 °C from each data point to turn the record into an anomaly relative the 1961–1990 baseline, then added 0.3134 °C to each data point to place this record on our 1850–1900 baseline.

Era6, **ΔT** is based on the isotopic composition of marine carbonates corrected for the influence of oceanic acidity and adjusted also for modeled variations of ancient, atmospheric CO_2 (Royer et al. 2004) archived at:

http://www.realclimate.org/docs/Temp-summary-from-Royer-et-al-2004.xls

Data in column D of this file were used. The authors have estimated changes in deep sea temperature relative to present. We have converted to surface temperature anomaly by multiplying their record by 2.5, the ratio of changes in global surface temperature to deep sea temperature according to equation 4.2 of Hansen et al. (2013). We have interpreted present to mean the 1961–1990 baseline, so we have also added 0.3134 °C to the data so that this record is also reflective of our 1850–1900 baseline.

Era 1, **CO_2** is based on three data records:

(i) 1980 to present: global, annual average CO_2 provided by the NOAA Earth System Research Laboratory (ESRL) (Ballantyne et al. 2012) at:
ftp://aftp.cmdl.noaa.gov/products/trends/co2/co2_annmean_gl.txt

(ii) 1765–1979: global, annual average CO_2 provided by the Potsdam Institute for Climate Research, developed as model inputs (Meinshausen et al. 2011) for climate model simulations used in the 2013 IPCC report, archived at:
http://www.pik-potsdam.de/~mmalte/rcps/data/RCP45_MIDYEAR_CONCENTRATIONS.DAT
This web address points to the RCP4.5 scenario, which is featured heavily in Chaps. 2 and 3 of this book. Since the record of CO_2 over this time period is constrained by observations, the numerical values of CO_2 for 1765–1979 are identical for all four RCP scenarios used in IPCC (2013).

(iii) 1000 ybp to 1764: The Law Dome Ice Core of record CO_2 (MacFarling Meure et al. 2006) archived by NOAA National Centers for Environmental Information (NECI) at:
http://www1.ncdc.noaa.gov/pub/data/paleo/icecore/antarctica/law/law2006.txt
This record is based on laboratory measurement of the CO_2 content of air pockets extracted from the upper part of the ice core, termed the firn layer.

Eras 2 and 3, **CO_2** is based on a merged ice core data set that combines measurements from seven ice cores archived at:
http://www1.ncdc.noaa.gov/pub/data/paleo/icecore/antarctica/antarctica2015co2.xls
This record is also based on laboratory measurement of CO_2 in air extracted from the ice (e.g., Petit et al. 1999). Column 2 of the CO2_Composite tab of the Excel file has been used; this composite is based on ten publications, all cited in the file.

Eras 4, **5**, **and 6**, **CO_2** is based on proxy estimates from five methods, originating from more than a hundred individual publications, summarized by Royer et al. (2012) and Peppe and Royer (2015). We have used a data file containing these observations sent to us by Dana Royer, senior author of these papers. Data for each proxy was first averaged, for all points falling within temporal bins of width 1 million years for Era 4, 5 million years for Era 5, and 50 million years for Era 5. Then, for each time bin, all available proxy means were averaged, resulting in the CO_2 time series connected by the blue lines. The error bars represent the minimum and maximum of the various proxy means available for specific time intervals. If CO_2 from a proxy was not available for a particular bin, a linear interpolation across adjacent time bins was applied, if possible. Otherwise, CO_2 from that missing proxy was treated as not available. The time ranges spanned by the five proxies are: paleosols (1–400 Mybp); alkenones (1–40 Mybp); stomata (1–400 Mypb); boron (1–15 and 35–55 Mybp); and liverworts (50–200 Mypb). Finally, the paleosol record as corrected by Breecker et al. (2009) was used.

Figure 1.2 shows values for the global mean surface temperature anomaly (ΔT) relative to the 1850–1900 baseline from two sources. For years prior to 1855, the proxy temperature time series of Jones and Mann (2004) was used. For 1855 to

present, instrument data from HadCRUT.4.4.0.0 (Jones et al. 2012) was used. Both datasets were downloaded from the websites described for Fig. 1.1. A 21-year running mean was used to smooth HadCRUT.4.4.0.0 record up to 2008; data from 2009 to 2015 represent unsmoothed annual averages.

The GHG data in Fig. 1.2 is based on three data records. For 0 AD to 1764, observations of CO_2, CH_4, and N_2O are based on the Law Dome Ice Core (MacFarling Meure et al. 2006) archived by NOAA NECI at:

http://www1.ncdc.noaa.gov/pub/data/paleo/icecore/antarctica/law/law2006.txt

For 1765 to modern times (1979 for CO_2; 1983 for CH_4, 1977 for N_2O), GHG abundances are based on the RCP 4.5 archive at:

http://www.pik-potsdam.de/~mmalte/rcps/data/RCP45_MIDYEAR_CONCENTRATIONS.DAT

For years since 1980 for CO_2, 1984 for CH_4, and 1978 for N_2O, GHG abundances are based on observations provided by NOAA ESRL (Ballantyne et al. 2012; Dlugokencky et al. 2009; Montzka et al. 2011) at:

ftp://aftp.cmdl.noaa.gov/products/trends/co2/co2_annmean_gl.txt

ftp://aftp.cmdl.noaa.gov/products/trends/ch4/ch4_annmean_gl.txt

ftp://ftp.cmdl.noaa.gov/hats/n2o/combined/HATS_global_N2O.txt

Population data in Fig. 1.2, for years up to and including 1950, are from the History Database of the Global Environment (HYDE) of the Netherlands Environmental Assessment Agency (Klein Goldewijk et al. 2010). For 1951 to present, population data from the Department of Economic and Social Affairs of the United Nations (United Nations 2015) have been used. The population databases are maintained at:

http://themasites.pbl.nl/tridion/en/themasites/hyde/index.html

http://esa.un.org/unpd/wpp/Download/Standard/Population

Figure 1.3 shows values of RF forcing of climate, relative to year 1765, for the RCP 4.5 scenario (Meinshausen et al. 2011) from file:

http://www.pik-potsdam.de/~mmalte/rcps/data/RCP45_MIDYEAR_RADFORCING.DAT

maintained at the Potsdam Institute for Climate Research. The Anthropogenic Aerosols terms includes the direct radiative effect of aerosols, the perturbation to the reflectivity of clouds induced by aerosols, and the darkening of snow caused by the deposition of black carbon. The following types of aerosols were considered: sulfate, organic carbon and black carbon from both fossil fuel combustion and biomass burning, nitrate, and mineral dust. The total anthropogenic term combines the contributions to RF of climate from all GHGs released by human activity, plus RF of climate due to aerosols, depletion of stratospheric O_3, the increase of tropospheric O_3, and rising surface reflectivity due to land use change. Figure 1.3 also shows the global mean surface temperature anomaly (ΔT) relative to pre-industrial (1850–1900) baseline. Data sources for ΔT are the same as for Fig. 1.2.

Figure 1.4 shows the change in the radiative forcing (ΔRF) over the course of the Anthropocene (in this case, 1750–2011) from Chap. 8 of IPCC (2013). Numerical estimates for ΔRF are shown when available; otherwise, numerical estimates for the change in Effective Radiative Forcing (ΔERF) are used. Effective Radiative Forcing (ERF) is a new concept introduced in IPCC (2013), based on model simulations that

Table 1.3 ΔRF values used in Fig. 1.4

Term	ΔRF (W m^{-2})	Range of ΔRF (W m^{-2})	Origin within Chap. 8 of IPCC (2013)
CO_2	1.82	1.63–2.01	Table 8.2, RF
CH_4	0.48	0.43–0.53	Table 8.2, RF
N_2O	0.17	0.14–0.20	Table 8.2, RF
ODS[a]	0.33	0.297–0.363	Table 8.2, RF
Other F-Gases[b]	0.03	0.027–0.033	Table 8.2, RF
Tropospheric O_3	0.4	0.2–0.6	Table 8.6, RF
Stratospheric O_3	−0.05	−0.15 to 0.05	Table 8.6, RF
Stratospheric H_2O[c]	0.07	0.02–0.12	Table 8.6, RF
Contrails and Contrail-Induced Cirrus	0.05	0.02–0.15	Table 8.6, ERF
Surface Reflectivity: Land Use Change	−0.15	−0.25 to −0.05	Table 8.6, RF
Surface Refl.: Black Carbon on Snow	0.04	0.02–0.09	Table 8.6, RF
Aerosol Direct Effect	−0.45	−0.95 to 0.05	Table 8.6, ERF
Aerosol-Cloud Interaction	−0.45	−1.2 to 0.0	Table 8.6, ERF
Total Anthropogenic	2.3	1.1–3.3	Table 8.6, ERF
Solar Irradiance	0.05	0.0–0.10	Table 8.6, RF

[a]The definition of Ozone Depleting Substances used in Chap. 8 of IPCC (2013) combines the RF of climate due to CFC-11, CFC-12, CFC-13, CFC-113, CFC-114, CFC-115, HCFC-141b, HCFC-142b, CH_3CCl_3, CCl_4, Halon-1211, and Halon-1301. The IPCC (2013) definition appears to neglect Halon-1202, Halon-2402, CH_3Cl, and CH_3Br. The ΔRF of these four compounds is quite small, less than 0.002 W m^{-2}, so Fig. 1.4 would look identical had these four gases been considered

[b]This term considers the RF of climate due to HFCs, PFCs, SF_6, and a few other long-lived fluorinated species. The IPCC (2013) definition combines the RF of climate due to HFC-23, HFC-32, HFC-125, HFC-134a, HFC-143a, HFC-152a, CF_4, C_2F_6, SF_6, SO_2F_6, and NF_3

[c]This term represents the RF of climate due to the increase in stratospheric H_2O driven by rising levels of tropospheric CH_4. It does not include radiative effects of changes in stratospheric H_2O that occur in response to global warming (Solomon et al. 2010)

allow physical variables within the troposphere to respond to perturbations, except for those ocean and sea ice variables. For computations of RF, all surface and tropospheric conditions are kept fixed. Quoting Box 8.1 of IPCC (2013), "the calculation of ERF requires longer simulations with more complex models than the calculation of RF, but the inclusion of the additional rapid adjustments makes ERF a better indicator of the eventual global mean temperature response, especially for aerosols". We have used a mixture of ΔRF and ΔERF values for Fig. 1.4 because this is all that is available from Chap. 8 of IPCC (2013). Table 1.3 provides numerical estimates of the value, uncertainty, and origin of the data used in Fig. 1.4. All uncertainties represent 5–95 % confidence intervals and are given as a range, rather than a plus and minus value, since some are asymmetric about the mean.

Figure 1.5 shows a profile of the change in temperature over the time period 1959–2012, based on radiosonde observations collected in the latitude range 30°S to 30°N (Sherwood and Nishant 2015). Data reflect the Iterative Universal Kriging

(IUKv2) processing. Results are displayed as a function of altitude, rather than pressure, using a standard climatology for altitude versus pressure of the tropical atmosphere. The tropopause has been placed at the altitude corresponding to a pressure of 100 hPa. The patterns of tropospheric warming, stratospheric cooling, and drop in the tropospheric lapse rate (i.e., more warming aloft than at the surface) illustrated in Fig. 1.5 are seen throughout the global atmosphere, in addition to the tropics (Sherwood and Nishant 2015).

Figure 1.6 shows CO_2 from Mauna Loa Observatory (Keeling et al. 1976) and global annual average CO_2 (Ballantyne et al. 2012) provided by NOAA ESRL at:

ftp://ftp.cmdl.noaa.gov/products/trends/co2/co2_mm_mlo.txt

ftp://ftp.cmdl.noaa.gov/products/trends/co2/co2_annmean_gl.txt

The global CO_2 record given at the above URL starts in 1980. We have extended this record back to 1959 using annual, global average CO_2 growth rates given at:

http://www.esrl.noaa.gov/gmd/ccgg/trends/global.html#global_growth

The data used to construct the CO_2 emissions from the combustion of fossil fuel (Boden et al. 2013) plus land use change (Houghton et al. 2012) (green bars, Fig. 1.6a) originate from file:

http://cdiac.ornl.gov/ftp/Global_Carbon_Project/Global_Carbon_Budget_2015_v1.1.xlsx

hosted by the Carbon Dioxide Information Analysis Center (CDIAC) at the US Department of Energy's (DOE) Oak Ridge National Laboratory (ORNL). This same file is also provided by the Global Carbon Budget at:

http://www.globalcarbonproject.org/carbonbudget/15/files/Global_Carbon_Budget_2015v1.1.xlsx

Contents of this file, which contains much more information than used here, are described by Le Quéré et al. (2015). The blue bars are found by multiplying the difference in annual average CO_2 mixing ratio, units of ppm, by 7.768, to arrive at the mass of CO_2 in Gt (see Le Quéré et al. (2015)). Finally, the Tropical Pacific ENSO index represents the anomaly of sea surface temperature in the region bounded by 20°S to 20°N latitude and 160°E to 80°W longitude, relative to a long-term climatology. Monthly values of this index have been computed as described by Zhang et al. (1997), using HadSST3.1.1.0 sea surface temperature data (Kennedy et al. 2011a, b) provided by the Hadley Centre of the United Kingdom Met Office in file:

http://hadobs.metoffice.com/hadsst3/data/HadSST.3.1.1.0/netcdf/HadSST.3.1.1.0.median_netcdf.zip

Figure 1.7 shows CO_2 (Keeling et al. 1976), the O_2/N_2 ratio (Keeling et al. 1996), and $\delta^{13}C$ of CO_2 (Keeling et al. 2005) from Mauna Loa Observatory (MLO) as well as CO_2 from the South Pole (SPO) (Tans et al. 1990). For CO_2, the solid black line shows monthly mean data from NOAA ESRL, based on the same file given in Methods for Fig. 1.6. Daily measurements of CO_2 at MLO (dots) are based on data provided by the Scripps Institution of Oceanography (SIO) of the University of California, San Diego at:

http://scrippsco2.ucsd.edu/assets/data/atmospheric/stations/flask_co2/daily/daily_flask_co2_mlo.csv

Monthly mean CO_2 at SPO (red line) is based on data provided by NOAA ESRL at:

http://scrippsco2.ucsd.edu/assets/data/atmospheric/stations/flask_co2/monthly/monthly_flask_co2_spo.csv

Monthly (line) and daily (dots) observations of the O_2/N_2 ratio are based on data archived by SIO at:

http://scrippso2.ucsd.edu/sites/default/files/data/o2_data/o2_monthly/mloo.txt

http://scrippso2.ucsd.edu/sites/default/files/data/o2_data/o2_daily/mlooav.csv

Finally, monthly (line) and daily (dots) $^{13}\delta CO_2$ is also based on data from SIO, at:

http://scrippsco2.ucsd.edu/assets/data/atmospheric/stations/flask_isotopic/monthly/monthly_flask_c13_mlo.csv

http://scrippsco2.ucsd.edu/assets/data/atmospheric/stations/flask_isotopic/daily/daily_flask_c13_mlo.csv

Figure 1.8 shows the difference between annual average CO_2 at MLO and CO_2 at SPO versus total anthropogenic emissions of CO_2. Here, we formed annual average CO_2 for each station from monthly mean values, based on in situ and flask sampling archived by SIO at:

http://scrippsco2.ucsd.edu/assets/data/atmospheric/stations/in_situ_co2/monthly/monthly_in_situ_co2_mlo.csv

http://scrippsco2.ucsd.edu/assets/data/atmospheric/stations/flask_co2/monthly/monthly_flask_co2_spo.csv

The total anthropogenic emissions of CO_2 are annual tabulations, reflecting the sum of combustion of fossil fuel (Boden et al. 2013) plus land use change (Houghton et al. 2012), and originate from the Global Carbon Project archive described in Methods for Fig. 1.6.

Figure 1.9 shows an estimate for the sources and sinks of atmospheric CH_4. Numerical values of the CH_4 source for total humans (335 Tg year^{-1}), total natural (218 Tg year^{-1}), natural wetlands (175 Tg year^{-1}), other natural (43 Tg year^{-1}) are from the top-down estimates for 2000–2009 given in Table 1 of Kirschke et al. (2013). The apportionment of the human sources is based on Fig. 1 of Conrad (2009). Numerical values of the total sink (550 Tg year^{-1}) and the sink due to soils (32 Tg year^{-1}) are also based on the top-down estimates from table 1 of Kirschke et al. (2013), whereas the sinks due to chemical loss via reactions with tropospheric OH (452.8 Tg year^{-1}), reactions with tropospheric Cl (21.4 Tg year^{-1}), and stratospheric chemistry (43.7 Tg year^{-1}) are based by scaling the bottom-up estimates of these quantities given in Table 1 of Kirschke et al. (2013) for the decade 2000–2009 by the ratio 518/604 = 0.8576, where 518 Tg year^{-1} is the total chemical sink found using the trop-down approach and 604 Tg year^{-1} is the total chemical sink found using the bottom-up approach. The numbers have been combined in this manner to provide a self-consistent estimate of the CH_4 source and sink terms by combining best available information from several studies and approaches.

Figure 1.10 shows ΔRF due to CO_2, CH_4, N_2O, and all anthropogenic GHGs from the RCP 4.5 scenario (Meinshausen et al. 2011). The numerical values have been obtained from the same file used to find ΔRF for Fig. 1.3. The figure also

shows 71 plausible scenarios for total ΔRF due to anthropogenic aerosols from Smith and Bond (2014). A data file containing the 71 time series for ΔRF of climate due to aerosols that appeared as Fig. 1.4 of this paper was sent to us by Steven J. Smith, corresponding author of this paper.

References

Anderson DC, Nicely JM, Salawitch RJ, Canty TP, Dickerson RR, Hanisco TF, Wolfe GM, Apel EC, Atlas E, Bannan T, Bauguitte S, Blake NJ, Bresch JF, Campos TL, Carpenter LJ, Cohen MD, Evans M, Fernandez RP, Kahn BH, Kinnison DE, Hall SR, Harris NRP, Hornbrook RS, Lamarque J-F, Le Breton M, Lee JD, Percival C, Pfister L, Pierce RB, Riemer DD, Saiz-Lopez A, Stunder BJB, Thompson AM, Ullmann K, Vaughan A, Weinheimer AJ (2016) A pervasive role for biomass burning in tropical high ozone/low water structures. Nat Commun 7, 10267. doi:10.1038/ncomms10267

Arnold T, Mühle J, Salameh PK, Harth CM, Ivy DJ, Weiss RF (2012) Automated measurement of nitrogen trifluoride in ambient air. Anal Chem 84(11):4798–4804. doi:10.1021/ac300373e

Ballantyne AP, Alden CB, Miller JB, Tans PP, White JWC (2012) Increase in observed net carbon dioxide uptake by land and oceans during the past 50 years. Nature 488(7409):70–72

Bard E, Raisbeck G, Yiou F, Jouzel J (2000) Solar irradiance during the last 1200 years based on cosmogenic nuclides. Tellus B 52(3):985–992. doi:10.1034/j.1600-0889.2000.d01-7.x

Barnola JM, Raynaud D, Korotkevich YS, Lorius C (1987) Vostok ice core provides 160,000-year record of atmospheric CO_2. Nature 329(6138):408–414

Bell ML, Dominici F, Keita E, Zeger SL, Samet JM (2007) Spatial and temporal variation in $PM_{2.5}$ chemical composition in the United States for health effects studies. Environ Health Perspect 115(7):989–995

Bera PP, Francisco JS, Lee TJ (2009) Identifying the molecular origin of global warming. J Phys Chem A 113(45):12694–12699. doi:10.1021/jp905097g

Berner RA (1997) The rise of plants and their effect on weathering and atmospheric CO_2. Science 276(5312):544–546. doi:10.1126/science.276.5312.544

Berner RA, Lasaga AC, Garrels RM (1983) The carbonate-silicate geochemical cycle and its effect on atmospheric carbon dioxide over the past 100 million years. Am J Sci 283(7):641–683. doi:10.2475/ajs.283.7.641

Boden TA, Marland G, Andres RJ (2013) Global, regional, and national fossil-fuel CO_2 emissions. doi:10.3334/CDIAC/00001_V2013

Bond TC, Doherty SJ, Fahey DW, Forster PM, Berntsen T, DeAngelo BJ, Flanner MG, Ghan S, Kärcher B, Koch D, Kinne S, Kondo Y, Quinn PK, Sarofim MC, Schultz MG, Schulz M, Venkataraman C, Zhang H, Zhang S, Bellouin N, Guttikunda SK, Hopke PK, Jacobson MZ, Kaiser JW, Klimont Z, Lohmann U, Schwarz JP, Shindell D, Storelvmo T, Warren SG, Zender CS (2013) Bounding the role of black carbon in the climate system: a scientific assessment. J Geophys Res Atmos 118(11):5380–5552. doi:10.1002/jgrd.50171

Bony S, Colman R, Kattsov VM, Allan RP, Bretherton CS, Dufresne J-L, Hall A, Hallegatte S, Holland MM, Ingram W, Randall DA, Doden BJ, Tselioudis G, Webb MJ (2006) How well do we understand and evaluate climate change feedback processes? J Clim 19:3445–3482. doi:10.1029/2005GL023851

Bousquet P, Peylin P, Ciais P, Le Quéré C, Friedlingstein P, Tans PP (2000) Regional changes in carbon dioxide fluxes of land and oceans since 1980. Science 290(5495):1342–1346. doi:10.1126/science.290.5495.1342

Brasier MD, Green OR, Jephcoat AP, Kleppe AK, Van Kranendonk MJ, Lindsay JF, Steele A, Grassineau NV (2002) Questioning the evidence for Earth's oldest fossils. Nature 416(6876):76–81. doi:10.1038/416076a

Breecker DO, Sharp ZD, McFadden LD (2009) Seasonal bias in the formation and stable isotopic composition of pedogenic carbonate in modern soils from central New Mexico, USA. GSA Bull 121(3–4):630–640. doi:10.1130/b26413.1

Brook EJ, Harder S, Severinghaus J, Steig EJ, Sucher CM (2000) On the origin and timing of rapid changes in atmospheric methane during the Last Glacial Period. Glob Biogeochem Cycles 14(2):559–572. doi:10.1029/1999GB001182

Caillon N, Severinghaus JP, Jouzel J, Barnola J-M, Kang J, Lipenkov VY (2003) Timing of atmospheric CO_2 and Antarctic temperature changes across termination III. Science 299(5613):1728–1731. doi:10.1126/science.1078758

Canfield DE, Raiswell R (1999) The evolution of the sulfur cycle. Am J Sci 299(7–9):697–723. doi:10.2475/ajs.299.7-9.697

Carslaw KS, Lee LA, Reddington CL, Pringle KJ, Rap A, Forster PM, Mann GW, Spracklen DV, Woodhouse MT, Regayre LA, Pierce JR (2013) Large contribution of natural aerosols to uncertainty in indirect forcing. Nature 503(7474):67–71. doi:10.1038/nature12674

Carto SL, Weaver AJ, Hetherington R, Lam Y, Wiebe EC (2009) Out of Africa and into an ice age: on the role of global climate change in the late Pleistocene migration of early modern humans out of Africa. J Hum Evol 56(2):139–151. doi:10.1016/j.jhevol.2008.09.004

Chylek P, Lohmann U (2005) Ratio of the Greenland to global temperature change: comparison of observations and climate modeling results. Geophys Res Lett 32(14), L14705. doi:10.1029/2005GL023552

Chylek P, Lohmann U (2008) Aerosol radiative forcing and climate sensitivity deduced from the Last Glacial Maximum to Holocene transition. Geophys Res Lett 35(4), L23703. doi:10.1029/2007GL032759

Conrad R (2009) The global methane cycle: recent advances in understanding the microbial processes involved. Environ Microbiol Rep 1(5):285–292. doi:10.1111/j.1758-2229.2009.00038.x

Crutzen PJ, Stoermer EF (2000) The Anthropocene. IGBP Newsletter, Royal Swedish Academy of Sciences, vol 41

Crutzen PJ, Mosier AR, Smith KA, Winiwarter W (2016) N_2O release from agro-biofuel production negates global warming reduction by replacing fossil fuels. In: Crutzen JP, Brauch GH (eds) Paul J. Crutzen: a pioneer on atmospheric chemistry and climate change in the anthropocene. Springer International Publishing, Cham, pp 227–238

Dessert C, Dupré B, François LM, Schott J, Gaillardet J, Chakrapani G, Bajpai S (2001) Erosion of Deccan Traps determined by river geochemistry: impact on the global climate and the 87Sr/86Sr ratio of seawater. Earth Planet Sci Lett 188(3–4):459–474, http://dx.doi.org/10.1016/S0012-821X(01)00317-X

Dlugokencky EJ, Bruhwiler L, White JWC, Emmons LK, Novelli PC, Montzka SA, Masarie KA, Lang PM, Crotwell AM, Miller JB, Gatti LV (2009) Observational constraints on recent increases in the atmospheric CH_4 burden. Geophys Res Lett 36(18), L18803. doi:10.1029/2009GL039780

Dominici F, Peng RD, Bell ML, Pham L, McDermott A, Zeger SL, Samet JM (2006) Fine particulate air pollution and hospital admission for cardiovascular and respiratory diseases. JAMA 295(10):1127–1134. doi:10.1001/jama.295.10.1127

Erb MP, Broccoli AJ, Clement AC (2013) The contribution of radiative feedbacks to orbitally driven climate change. J Clim 26(16):5897–5914. doi:10.1175/JCLI-D-12-00419.1

Fan S-M, Blaine TL, Sarmiento JL (1999) Terrestrial carbon sink in the Northern Hemisphere estimated from the atmospheric CO_2 difference between Mauna Loa and the South Pole since 1959. Tellus B 51(5):863–870. doi:10.1034/j.1600-0889.1999.t01-4-00001.x

Frei R, Gaucher C, Poulton SW, Canfield DE (2009) Fluctuations in Precambrian atmospheric oxygenation recorded by chromium isotopes. Nature 461(7261):250–253. doi:10.1038/nature08266

Galloway JN, Winiwarter W, Leip A, Leach AM, Bleeker A, Erisman JW (2014) Nitrogen footprints: past, present and future. Environ Res Lett 9(11):115003

Gepts P, Papa R (2001) Evolution during domestication. In: Encyclopedia of life sciences. Wiley, New York. doi:10.1038/npg.els.0003071

Gerlach T (2011) Volcanic versus anthropogenic carbon dioxide. Eos 92(24):201–208
Hansen J, Sato M, Russell G, Kharecha P (2013) Climate sensitivity, sea level and atmospheric carbon dioxide. Philos Trans R Soc Lond A Math Phys Eng Sci 371(2001). doi:10.1098/rsta.2012.0294
Hay WW, Barron EJ, Thompson SL (1990) Global atmospheric circulation experiments on an Earth with polar and tropical continents. J Geol Soc 147(5):749–757. doi:10.1144/gsjgs.147.5.0749
He H, Vinnikov KY, Li C, Krotkov NA, Jongeward AR, Li Z, Stehr JW, Hains JC, Dickerson RR (2016) Response of SO_2 and particulate air pollution to local and regional emission controls: a case study in Maryland. Earth's Future 4(4):94–109. doi:10.1002/2015EF000330
Houghton RA, House JI, Pongratz J, van der Werf GR, DeFries RS, Hansen MC, Le Quéré C, Ramankutty N (2012) Carbon emissions from land use and land-cover change. Biogeosciences 9(12):5125–5142. doi:10.5194/bg-9-5125-2012
Imbrie J, Imbrie KP (1979) Ice ages: solving the mystery. Harvard University Press, Cambridge, MA
IPCC (1995) Climate change 1995: the science of climate change. Contribution of working group I to the second assessment report of the intergovernmental panel on climate change. Cambridge, UK and New York, NY, USA
IPCC (2001) Climate change 2001: the scientific basis. contribution of working group I to the third assessment report of the intergovernmental panel on climate change. Cambridge, UK and New York, NY, USA
IPCC (2007) Climate change 2007: the physical science basis. Contribution of working group I to the fourth assessment report of the intergovernmental panel on climate change. Cambridge, UK and New York, NY, USA
IPCC (2013) Climate change 2013: the physical science basis. Contribution of working group I to the fifth assessment report of the intergovernmental panel on climate change. Cambridge, UK and New York, NY, USA
IPCC/TEAP (2005) Safeguarding the ozone layer and the global climate systems: issues related to hydrofluorocarbons and perfluorocarbons. Prepared by Working Group I and III of the Intergovernmental Panel on Climate Change, and the Technology and Economic Assessment Panel. Cambridge, UK and New York, NY, USA
Jimenez JL, Canagaratna MR, Donahue NM, Prevot AS, Zhang Q, Kroll JH, DeCarlo PF, Allan JD, Coe H, Ng NL, Aiken AC, Docherty KS, Ulbrich IM, Grieshop AP, Robinson AL, Duplissy J, Smith JD, Wilson KR, Lanz VA, Hueglin C, Sun YL, Tian J, Laaksonen A, Raatikainen T, Rautiainen J, Vaattovaara P, Ehn M, Kulmala M, Tomlinson JM, Collins DR, Cubison MJ, Dunlea EJ, Huffman JA, Onasch TB, Alfarra MR, Williams PI, Bower K, Kondo Y, Schneider J, Drewnick F, Borrmann S, Weimer S, Demerjian K, Salcedo D, Cottrell L, Griffin R, Takami A, Miyoshi T, Hatakeyama S, Shimono A, Sun JY, Zhang YM, Dzepina K, Kimmel JR, Sueper D, Jayne JT, Herndon SC, Trimborn AM, Williams LR, Wood EC, Middlebrook AM, Kolb CE, Baltensperger U, Worsnop DR (2009) Evolution of organic aerosols in the atmosphere. Science 326(5959):1525–1529. doi:10.1126/science.1180353
Johanson D, White T (1979) A systematic assessment of early African hominids. Science 203(4378):321–330. doi:10.1126/science.104384
Jones PD, Mann ME (2004) Climate over past millennia. Rev Geophys 42(2):RG2002. doi:10.1029/2003RG000143
Jones PD, Lister DH, Osborn TJ, Harpham C, Salmon M, Morice CP (2012) Hemispheric and large-scale land-surface air temperature variations: an extensive revision and an update to 2010. J Geophys Res 117(D5):D05127. doi:10.1029/2011jd017139
Jouzel J, Lorius C, Petit JR, Genthon C, Barkov NI, Kotlyakov VM, Petrov VM (1987) Vostok ice core: a continuous isotope temperature record over the last climatic cycle (160,000 years). Nature 329(6138):403–408
Jouzel J, Masson-Delmotte V, Cattani O, Dreyfus G, Falourd S, Hoffmann G, Minster B, Nouet J, Barnola JM, Chappellaz J, Fischer H, Gallet JC, Johnsen S, Leuenberger M, Loulergue L, Luethi D, Oerter H, Parrenin F, Raisbeck G, Raynaud D, Schilt A, Schwander J, Selmo E, Souchez R, Spahni R, Stauffer B, Steffensen JP, Stenni B, Stocker TF, Tison JL, Werner M,

Wolff EW (2007) Orbital and millennial Antarctic climate variability over the past 800,000 years. Science 317(5839):793–796. doi:10.1126/science.1141038

Kahn RA (2012) Reducing the uncertainties in direct aerosol radiative forcing. Surv Geophys 33(3):701–721. doi:10.1007/s10712-011-9153-z

Kasting JF, Siefert JL (2002) Life and the evolution of Earth's atmosphere. Science 296(5570):1066–1068. doi:10.1126/science.1071184

Keeling CD, Bacastow RB, Bainbridge AE, Ekdahl CA, Guenther PR, Waterman LS, Chin JFS (1976) Atmospheric carbon dioxide variations at Mauna Loa Observatory, Hawaii. Tellus 28(6):538–551. doi:10.1111/j.2153-3490.1976.tb00701.x

Keeling RF, Piper SC, Heimann M (1996) Global and hemispheric CO_2 sinks deduced from changes in atmospheric O_2 concentration. Nature 381(6579):218–221

Keeling CD, Piper SC, Bacastow RB, Wahlen M, Whorf TP, Heimann M, Meijer HA (2005) Atmospheric CO_2 and $^{13}CO_2$ exchange with the terrestrial biosphere and oceans from 1978 to 2000: observations and carbon cycle implications. In: Baldwin IT, Caldwell MM, Heldmaier G et al (eds) A history of atmospheric CO_2 and its effects on plants, animals, and ecosystems. Springer, New York, pp 83–113. doi:10.1007/0-387-27048-5_5

Kennedy JJ, Rayner NA, Smith RO, Parker DE, Saunby M (2011a) Reassessing biases and other uncertainties in sea-surface temperature observations measured in situ since 1850, Part 1: Measurement and sampling uncertainties. J Geophys Res 116:D14103. doi:10.1029/2010JD015218

Kennedy JJ, Rayner NA, Smith RO, Parker DE, Saunby M (2011b) Reassessing biases and other uncertainties in sea-surface temperature observations measured in situ since 1850, Part 2: Biases and homogenisation. J Geophys Res 116, D14104. doi:10.1029/2010JD01522

Kenrick P, Crane PR (1997) The origin and early evolution of plants on land. Nature 389(6646):33–39

Keywood M, Kanakidou M, Stohl A, Dentener F, Grassi G, Meyer CP, Torseth K, Edwards D, Thompson AM, Lohmann U, Burrows J (2013) Fire in the air: biomass burning impacts in a changing climate. Crit Rev Environ Sci Technol 43(1):40–83. doi:10.1080/10643389.2011.604248

Kirschke S, Bousquet P, Ciais P, Saunois M, Canadell JG, Dlugokencky EJ, Bergamaschi P, Bergmann D, Blake DR, Bruhwiler L, Cameron-Smith P, Castaldi S, Chevallier F, Feng L, Fraser A, Heimann M, Hodson EL, Houweling S, Josse B, Fraser PJ, Krummel PB, Lamarque J-F, Langenfelds RL, Le Quere C, Naik V, O'Doherty S, Palmer PI, Pison I, Plummer D, Poulter B, Prinn RG, Rigby M, Ringeval B, Santini M, Schmidt M, Shindell DT, Simpson IJ, Spahni R, Steele LP, Strode SA, Sudo K, Szopa S, van der Werf GR, Voulgarakis A, van Weele M, Weiss RF, Williams JE, Zeng G (2013) Three decades of global methane sources and sinks. Nat Geosci 6(10):813–823. doi:10.1038/ngeo1955, http://www.nature.com/ngeo/journal/v6/n10/abs/ngeo1955.html#supplementary-information

Klein Goldewijk K, Beusen A, Janssen P (2010) Long-term dynamic modeling of global population and built-up area in a spatially explicit way: HYDE 3.1. The Holocene 20(4):565–573. doi:10.1177/0959683609356587

Koven CD, Ringeval B, Friedlingstein P, Ciais P, Cadule P, Khvorostyanov D, Krinner G, Tarnocai C (2011) Permafrost carbon-climate feedbacks accelerate global warming. Proc Natl Acad Sci 108(36):14769–14774. doi:10.1073/pnas.1103910108

Krotkov NA, McLinden CA, Li C, Lamsal LN, Celarier EA, Marchenko SV, Swartz WH, Bucsela EJ, Joiner J, Duncan BN, Boersma KF, Veefkind JP, Levelt PF, Fioletov VE, Dickerson RR, He H, Lu Z, Streets DG (2016) Aura OMI observations of regional SO_2 and NO_2 pollution changes from 2005 to 2015. Atmos Chem Phys 16(7):4605–4629. doi:10.5194/acp-16-4605-2016

Kvenvolden KA (1993) Gas hydrates—geological perspective and global change. Rev Geophys 31(2):173–187. doi:10.1029/93RG00268

Lacis AA, Mischenko MI (1995) Climate forcing, climate sensitivity, and climate response: a radiative modeling perspective on atmospheric aerosols. Aerosol forcing of climate: report of the Dahlem workshop on aerosol forcing of climate. Chichester, England/New York

Le Quéré C (2010) Trends in the land and ocean carbon uptake. Curr Opin Environ Sustain 2(4):219–224, http://dx.doi.org/10.1016/j.cosust.2010.06.003

Le Quéré C, Aumont O, Bopp L, Bousquet P, Ciais P, Francey R, Heimann M, Keeling CD, Keeling RF, Kheshgi H, Peylin P, Piper SC, Prentice IC, Rayner PJ (2003) Two decades of ocean CO_2 sink and variability. Tellus B 55(2):649–656. doi:10.1034/j.1600-0889.2003.00043.x

Le Quéré C, Moriarty R, Andrew RM, Canadell JG, Sitch S, Korsbakken JI, Friedlingstein P, Peters GP, Andres RJ, Boden TA, Houghton RA, House JI, Keeling RF, Tans P, Arneth A, Bakker DCE, Barbero L, Bopp L, Chang J, Chevallier F, Chini LP, Ciais P, Fader M, Feely RA, Gkritzalis T, Harris I, Hauck J, Ilyina T, Jain AK, Kato E, Kitidis V, Klein Goldewijk K, Koven C, Landschützer P, Lauvset SK, Lefèvre N, Lenton A, Lima ID, Metzl N, Millero F, Munro DR, Murata A, Nabel JEMS, Nakaoka S, Nojiri Y, O'Brien K, Olsen A, Ono T, Pérez FF, Pfeil B, Pierrot D, Poulter B, Rehder G, Rödenbeck C, Saito S, Schuster U, Schwinger J, Séférian R, Steinhoff T, Stocker BD, Sutton AJ, Takahashi T, Tilbrook B, van der Laan-Luijkx IT, van der Werf GR, van Heuven S, Vandemark D, Viovy N, Wiltshire A, Zaehle S, Zeng N (2015) Global carbon budget 2015. Earth Syst Sci Data 7(2):349–396. doi:10.5194/essd-7-349-2015

Loulergue L, Schilt A, Spahni R, Masson-Delmotte V, Blunier T, Lemieux B, Barnola J-M, Raynaud D, Stocker TF, Chappellaz J (2008) Orbital and millennial-scale features of atmospheric CH_4 over the past 800,000 years. Nature 453(7193):383–386, http://www.nature.com/nature/journal/v453/n7193/suppinfo/nature06950_S1.html

Lunt DJ, Foster GL, Haywood AM, Stone EJ (2008) Late Pliocene Greenland glaciation controlled by a decline in atmospheric CO_2 levels. Nature 454(7208):1102–1105. doi:10.1038/nature07223

MacFarling Meure C, Etheridge D, Trudinger C, Steele P, Langenfelds R, van Ommen T, Smith A, Elkins J (2006) Law Dome CO_2, CH_4 and N_2O ice core records extended to 2000 years BP. Geophys Res Lett 33(14). doi:10.1029/2006GL026152

Mann ME (2012) The hockey stick and the climate wars: dispatches from the front lines. Columbia University Press, Columbia

Mann ME, Bradley RS, Hughes MK (1999) Northern hemisphere temperatures during the past millennium: inferences, uncertainties, and limitations. Geophys Res Lett 26(6):759–762. doi:10.1029/1999GL900070

Margulis L, Sagan D (1986) Microcosmos: four billion years of evolution from our microbial ancestors. University of California Press, Berkeley, CA

Marino BD, McElroy MB, Salawitch RJ, Spaulding WG (1992) Glacial to interglacial variations in the carbon isotopic composition of atmospheric CO_2. Nature 357:461–466

Martin JH (1990) Glacial-interglacial CO_2 change: the iron hypothesis. Paleoceanography 5(1):1–13. doi:10.1029/PA005i001p00001

Marty B, Tolstikhin IN (1998) CO_2 fluxes from mid-ocean ridges, arcs and plumes. Chem Geol 145(3–4):233–248. http://dx.doi.org/10.1016/S0009-2541(97)00145-9

Mason BG, Pyle DM, Oppenheimer C (2004) The size and frequency of the largest explosive eruptions on Earth. Bull Volcanol 66(8):735–748. doi:10.1007/s00445-004-0355-9

Masson-Delmotte V, Kageyama M, Braconnot P, Charbit S, Krinner G, Ritz C, Guilyardi E, Jouzel J, Abe-Ouchi A, Crucifix M, Gladstone RM, Hewitt CD, Kitoh A, LeGrande AN, Marti O, Merkel U, Motoi T, Ohgaito R, Otto-Bliesner B, Peltier WR, Ross I, Valdes PJ, Vettoretti G, Weber SL, Wolk F, Yu Y (2006) Past and future polar amplification of climate change: climate model intercomparisons and ice-core constraints. Clim Dyn 26(5):513–529. doi:10.1007/s00382-005-0081-9

McLinden CA, Fioletov V, Shephard MW, Krotkov N, Li C, Martin RV, Moran MD, Joiner J (2016) Space-based detection of missing sulfur dioxide sources of global air pollution. Nat Geosci 9(7):496–500. doi:10.1038/ngeo2724, http://www.nature.com/ngeo/journal/vaop/ncurrent/abs/ngeo2724.html#supplementary-information

Meinshausen M, Smith SJ, Calvin K, Daniel JS, Kainuma MLT, Lamarque JF, Matsumoto K, Montzka SA, Raper SCB, Riahi K, Thomson A, Velders GJM, Vuuren DPP (2011) The RCP greenhouse gas concentrations and their extensions from 1765 to 2300. Clim Chang 109(1–2):213–241. doi:10.1007/s10584-011-0156-z

Minschwaner K, Salawitch R, McElroy M (1993) Absorption of solar radiation by O_2: implications for O_3 and lifetimes of N_2O, $CFCl_3$, and CF_2Cl_2. J Geophys Res 98(D6):10543–10561

Mitchell DM (2016) Attributing the forced components of observed stratospheric temperature variability to external drivers. Q J R Meteorol Soc 142(695):1041–1047. doi:10.1002/qj.2707

Moberg A, Sonechkin DM, Holmgren K, Datsenko NM, Karlen W (2005) Highly variable Northern Hemisphere temperatures reconstructed from low- and high-resolution proxy data. Nature 433(7026):613–617. doi:10.1038/nature03265

Montzka SA, Dlugokencky EJ, Butler JH (2011) Non-CO_2 greenhouse gases and climate change. Nature 476(7358):43–50

Morgan MG, Adams PJ, Keith DW (2006) Elicitation of expert judgments of aerosol forcing. Clim Chang 75(1–2):195–214. doi:10.1007/s10584-005-9025-y

Mühle J, Ganesan AL, Miller BR, Salameh PK, Harth CM, Greally BR, Rigby M, Porter LW, Steele LP, Trudinger CM, Krummel PB, O'Doherty S, Fraser PJ, Simmonds PG, Prinn RG, Weiss RF (2010) Perfluorocarbons in the global atmosphere: tetrafluoromethane, hexafluoroethane, and octafluoropropane. Atmos Chem Phys 10(11):5145–5164. doi:10.5194/acp-10-5145-2010

Myhre G (2009) Consistency between satellite-derived and modeled estimates of the direct aerosol effect. Science 325(5937):187–190. doi:10.1126/science.1174461

NAS (2006) Surface temperature reconstructions for the last 2,000 years. The National Academies Press, National Academy of Sciences

Newhall CG, Self S (1982) The volcanic explosivity index (VEI) an estimate of explosive magnitude for historical volcanism. J Geophys Res Oceans 87(C2):1231–1238. doi:10.1029/JC087iC02p01231

Parrenin F, Masson-Delmotte V, Köhler P, Raynaud D, Paillard D, Schwander J, Barbante C, Landais A, Wegner A, Jouzel J (2013) Synchronous change of atmospheric CO_2 and Antarctic temperature during the last deglacial warming. Science 339(6123):1060–1063. doi:10.1126/science.1226368

Peppe DJ, Royer DL (2015) Can climate feel the pressure? Science 348(6240):1210–1211. doi:10.1126/science.aac5264

Petit JR, Jouzel J, Raynaud D, Barkov NI, Barnola JM, Basile I, Bender M, Chappellaz J, Davis M, Delaygue G, Delmotte M, Kotlyakov VM, Legrand M, Lipenkov VY, Lorius C, Pepin L, Ritz C, Saltzman E, Stievenard M (1999) Climate and atmospheric history of the past 420,000 years from the Vostok ice core, Antarctica. Nature 399(6735):429–436. http://www.nature.com/nature/journal/v399/n6735/suppinfo/399429a0_S1.html

Pierrehumbert RT (2014) Short-lived climate pollution. Annu Rev Earth Planet Sci 42(1):341–379. doi:10.1146/annurev-earth-060313-054843

Prather MJ, Hsu J (2008) NF_3, the greenhouse gas missing from Kyoto. Geophys Res Lett 35(12), L12810. doi:10.1029/2008GL034542

Prather MJ, Holmes CD, Hsu J (2012) Reactive greenhouse gas scenarios: systematic exploration of uncertainties and the role of atmospheric chemistry. Geophys Res Lett 39(9). doi:10.1029/2012GL051440

Randerson JT, van der Werf GR, Collatz GJ, Giglio L, Still CJ, Kasibhatla P, Miller JB, White JWC, DeFries RS, Kasischke ES (2005) Fire emissions from C3 and C4 vegetation and their influence on interannual variability of atmospheric CO2 and δ13CO2. Global Biogeochem Cycles 19(2). doi:10.1029/2004GB002366

Ravishankara AR, Daniel JS, Portmann RW (2009) Nitrous oxide (N_2O): the dominant ozone-depleting substance emitted in the 21st century. Science 326(5949):123–125. doi:10.1126/science.1176985

Raymo ME, Ruddiman WF (1992) Tectonic forcing of late Cenozoic climate. Nature 359(6391):117–122

Revell LE, Tummon F, Salawitch RJ, Stenke A, Peter T (2015) The changing ozone depletion potential of N_2O in a future climate. Geophys Res Lett 42(22):10,047–10,055. doi:10.1002/2015GL065702

Revelle R, Suess HE (1957) Carbon dioxide exchange between atmosphere and ocean and the question of an increase of atmospheric CO_2 during the past decades. Tellus 9(1):18–27. doi:10.1111/j.2153-3490.1957.tb01849.x

Rigby M, Mühle J, Miller BR, Prinn RG, Krummel PB, Steele LP, Fraser PJ, Salameh PK, Harth CM, Weiss RF, Greally BR, O'Doherty S, Simmonds PG, Vollmer MK, Reimann S, Kim J, Kim KR, Wang HJ, Olivier JGJ, Dlugokencky EJ, Dutton GS, Hall BD, Elkins JW (2010) History of atmospheric SF_6 from 1973 to 2008. Atmos Chem Phys 10(21):10305–10320. doi:10.5194/acp-10-10305-2010

Rizzo AL, Jost H-J, Caracausi A, Paonita A, Liotta M, Martelli M (2014) Real-time measurements of the concentration and isotope composition of atmospheric and volcanic CO_2 at Mount Etna (Italy). Geophys Res Lett 41(7):2382–2389. doi:10.1002/2014GL059722

Rosenthal Y, Linsley BK, Oppo DW (2013) Pacific ocean heat content during the past 10,000 years. Science 342(6158):617–621. doi:10.1126/science.1240837

Royer DL, Berner RA, Montanez IP, Tabor NJ, Beerling DJ (2004) CO_2 as a primary driver of Phanerozoic climate. Geol Soc Am Today 14:4–10. doi:10.1130/1052-5173(2004)014<4:CAAPDO>2.0.CO;2

Royer DL, Pagani M, Beerling DJ (2012) Geobiological constraints on Earth system sensitivity to CO_2 during the Cretaceous and Cenozoic. Geobiology 10(4):298–310. doi:10.1111/j.1472-4669.2012.00320.x

Ruddiman WF (2003) The anthropogenic greenhouse era began thousands of years ago. Clim Chang 61(3):261–293. doi:10.1023/B:CLIM.0000004577.17928.fa

Sagan C, Mullen G (1972) Earth and mars: evolution of atmospheres and surface temperatures. Science 177(4043):52–56. doi:10.1126/science.177.4043.52

Santer BD, Painter JF, Bonfils C, Mears CA, Solomon S, Wigley TM, Gleckler PJ, Schmidt GA, Doutriaux C, Gillett NP, Taylor KE, Thorne PW, Wentz FJ (2013a) Human and natural influences on the changing thermal structure of the atmosphere. Proc Natl Acad Sci U S A 110(43):17235–17240. doi:10.1073/pnas.1305332110

Santer BD, Painter JF, Mears CA, Doutriaux C, Caldwell P, Arblaster JM, Cameron-Smith PJ, Gillett NP, Gleckler PJ, Lanzante J, Perlwitz J, Solomon S, Stott PA, Taylor KE, Terray L, Thorne PW, Wehner MF, Wentz FJ, Wigley TM, Wilcox LJ, Zou CZ (2013b) Identifying human influences on atmospheric temperature. Proc Natl Acad Sci U S A 110(1):26–33. doi:10.1073/pnas.1210514109

Schneider SH (1984) The coevolution of climate and life. Sierra Club Books, San Francisco

Self S, Widdowson M, Thordarson T, Jay AE (2006) Volatile fluxes during flood basalt eruptions and potential effects on the global environment: a Deccan perspective. Earth Planet Sci Lett 248(1–2):518–532, http://dx.doi.org/10.1016/j.epsl.2006.05.041

Sherwood SC, Nishant N (2015) Atmospheric changes through 2012 as shown by iteratively homogenized radiosonde temperature and wind data (IUKv2). Environ Res Lett 10(5):054007

Shindell DT, Faluvegi G (2009) Climate response to regional radiative forcing during the twentieth century. Nat Geosci 2(4):294–300, http://www.nature.com/ngeo/journal/v2/n4/suppinfo/ngeo473_S1.html

Shindell DT, Faluvegi G, Koch DM, Schmidt GA, Unger N, Bauer SE (2009) Improved attribution of climate forcing to emissions. Science 326(5953):716–718. doi:10.1126/science.1174760

Siegenthaler U, Oeschger H (1987) Biospheric CO_2 emissions during the past 200 years reconstructed by deconvolution of ice core data. Tellus B 39B(1–2):140–154. doi:10.1111/j.1600-0889.1987.tb00278.x

Smith SJ, Bond TC (2014) Two hundred fifty years of aerosols and climate: the end of the age of aerosols. Atmos Chem Phys 14(2):537–549. doi:10.5194/acp-14-537-2014

Smith KA, McTaggart IP, Tsuruta H (1997) Emissions of N_2O and NO associated with nitrogen fertilization in intensive agriculture, and the potential for mitigation. Soil Use Manag 13:296–304. doi:10.1111/j.1475-2743.1997.tb00601.x

Solomon S, Rosenlof KH, Portmann RW, Daniel JS, Davis SM, Sanford TJ, Plattner G-K (2010) Contributions of stratospheric water vapor to decadal changes in the rate of global warming. Science 327:1219–1223. doi:10.1126/science.1182488

Soon W, Baliunas S (2003) Proxy climatic and environmental changes of the past 1000 years. Clim Res 23(2):89–110

Sowers T (2006) Late Quaternary atmospheric CH_4 isotope record suggests marine clathrates are stable. Science 311(5762):838–840. doi:10.1126/science.1121235

Steffen W, Broadgate W, Deutsch L, Gaffney O, Ludwig C (2015) The trajectory of the Anthropocene: the great acceleration. Anthropocene Rev 2(1):81–98. doi:10.1177/2053019614564785

Streets DG, Canty T, Carmichael GR, de Foy B, Dickerson RR, Duncan BN, Edwards DP, Haynes JA, Henze DK, Houyoux MR, Jacobi DJ, Krotkov NA, Lamsal LN, Liu Y, Lu Z, Martini RV, Pfister GG, Pinder RW, Salawitch RJ, Wechti KJ (2013) Emissions estimation from satellite retrievals: a review of current capability. Atmos Environ 77:1011–1042. doi:10.1016/j.atmosenv.2013.05.051

Sturges WT, Wallington TJ, Hurley MD, Shine KP, Sihra K, Engel A, Oram DE, Penkett SA, Mulvaney R, Brenninkmeijer CAM (2000) A potent greenhouse gas identified in the atmosphere: SF_5CF_3. Science 289(5479):611–613. doi:10.1126/science.289.5479.611

Sturges WT, Oram DE, Laube JC, Reeves CE, Newland MJ, Hogan C, Martinerie P, Witrant E, Brenninkmeijer CAM, Schuck TJ, Fraser PJ (2012) Emissions halted of the potent greenhouse gas SF_5CF_3. Atmos Chem Phys 12(8):3653–3658. doi:10.5194/acp-12-3653-2012

Tans PP, Fung IY, Takahashi T (1990) Observational constraints on the global atmospheric CO_2 budget. Science 247(4949):1431–1438. doi:10.1126/science.247.4949.1431

Thomas NJ, Chang N-B, Qi C (2012) Preliminary assessment for global warming potential of leading contributory gases from a 40-in. LCD flat-screen television. Int J Life Cycle Assess 17(1):96–104. doi:10.1007/s11367-011-0341-3

Thomson AM, Calvin KV, Smith SJ, Kyle GP, Volke A, Patel P, Delgado-Arias S, Bond-Lamberty B, Wise MA, Clarke LE, Edmonds JA (2011) RCP4.5: a pathway for stabilization of radiative forcing by 2100. Clim Chang 109(1–2):77–94. doi:10.1007/s10584-011-0151-4

Tsai W-T (2008) Environmental and health risk analysis of nitrogen trifluoride (NF_3), a toxic and potent greenhouse gas. J Hazard Mater 159(2–3):257–263, http://dx.doi.org/10.1016/j.jhazmat.2008.02.023

United Nations (2015) World population prospects: the 2015 revision, methodology of the United Nations Population estimates and projections. Working Paper No. ESA/P/WP.242. New York, USA

Velders GJ, Andersen SO, Daniel JS, Fahey DW, McFarland M (2007) The importance of the Montreal Protocol in protecting climate. Proc Natl Acad Sci U S A 104(12):4814–4819. doi:10.1073/pnas.0610328104

Velders GJ, Fahey DW, Daniel JS, McFarland M, Andersen SO (2009) The large contribution of projected HFC emissions to future climate forcing. Proc Natl Acad Sci U S A 106(27):10949–10954. doi:10.1073/pnas.0902817106

Whiticar MJ (1996) Stable isotope geochemistry of coals, humic kerogens and related natural gases. Int J Coal Geol 32(1–4):191–215, http://dx.doi.org/10.1016/S0166-5162(96)00042-0

WMO (2014) World meteorological organization, scientific assessment of ozone depletion: 2014. Global Ozone Research and Monitoring Project—Report #55. Geneva, Switzerland

Yoon J, Burrows JP, Vountas M, von Hoyningen-Huene W, Chang DY, Richter A, Hilboll A (2014) Changes in atmospheric aerosol loading retrieved from space-based measurements during the past decade. Atmos Chem Phys 14(13):6881–6902. doi:10.5194/acp-14-6881-2014

Yoon J, Pozzer A, Chang DY, Lelieveld J, Kim J, Kim M, Lee YG, Koo JH, Lee J, Moon KJ (2016) Trend estimates of AERONET-observed and model-simulated AOTs between 1993 and 2013. Atmos Environ 125(Part A):33–47. http://dx.doi.org/10.1016/j.atmosenv.2015.10.058

Zeng N, Mariotti A, Wetzel P (2005) Terrestrial mechanisms of interannual CO_2 variability. Global Biogeochem Cycles 19(1). doi:10.1029/2004GB002273

Zhang Y, Wallace JM, Battisti DS (1997) ENSO-like interdecadal variability: 1900–93. J Clim 10:1004–1020

Zhang H, Wu JX, Shen ZP (2011) Radiative forcing and global warming potential of perfluorocarbons and sulfur hexafluoride. Sci China Earth Sci 54(5):764–772. doi:10.1007/s11430-010-4155-0

Zhu Z, Piao S, Myneni RB, Huang M, Zeng Z, Canadell JG, Ciais P, Sitch S, Friedlingstein P, Arneth A, Cao C, Cheng L, Kato E, Koven C, Li Y, Lian X, Liu Y, Liu R, Mao J, Pan Y, Peng S, Penuelas J, Poulter B, Pugh TAM, Stocker BD, Viovy N, Wang X, Wang Y, Xiao Z, Yang H, Zaehle S, Zeng N (2016) Greening of the Earth and its drivers. Nat Clim Change 6:791–795. doi:10.1038/nclimate3004, http://www.nature.com/nclimate/journal/vaop/ncurrent/abs/nclimate3004.html#supplementary-information